Highlights

The EPS contents in sediment with clams were significant higher

The near-bed in situ floc size was 70% larger over the clam flat

Flocculation processes were related to biological, SSC and turbulent influence

A comparison study on the sediment flocculation process between a bare tidal flat and a clam aquaculture mudflat: the important role of sediment concentration and biological processes

Jiasheng Li[1,2], Xindi Chen[3], Ian Townend[4], Benwei Shi[5] *, Jiabi Du[6], Jianhua Gao[1], Xiaowei Chuai[1], Zheng Gong[3], Ya Ping Wang[1,5] *

[1] *Ministry of Education Key Laboratory for Coast and Island Development, School of Geographic & Oceanographic Sciences, Nanjing University, Nanjing, 210093, China*

[2] *Key Laboratory of Oceanic and Polar Fisheries, Ministry of Agriculture and Rural Affairs; East China Sea Fisheries Research Institute, Chinese Academy of Fishery Sciences, Shanghai, 200090, China*

[3] *State Key Laboratory of Hydrology – Water Resources and Hydraulic Engineering, Hohai University, Nanjing, China*

[4] *School of Ocean and Earth Sciences, University of Southampton, United Kingdom*

[5] *State Key Laboratory of Estuarine and Coastal Research, East China Normal University, Shanghai 200062, China*

[6] *Department of Marine Sciences, Texas A&M University at Galveston, Galveston, TX 77554, United States*

Corresponding author information,

Telephone: 086-25-83686010;

Fax: 086-25-83595387;

Email address: ypwang@nju.edu.cn (Y. P. Wang); bwshi@sklec.ecnu.edu.cn（B.W. Shi）

Abstract

The flocculation process of cohesive sediment impacts upon estuaries and tidal flats by affecting the sediment dynamics, modifying the biogeochemical exchanges, and playing an essential role in coastal ecosystems and geomorphologic evolution. To understand the roles of biological activity on flocculation processes in aquaculture areas, here we undertook *in situ* measurements over a bare tidal flat and a nearby clam aquaculture mudflat on the Jiangsu coast, China. Near-bed *in situ* floc size, the grain size distribution of suspended particles in seawater, suspended sediment concentration (SSC), and currents were obtained for nine consecutive semidiurnal tidal cycles simultaneously at the two sites. Correlation analysis indicated that the flocculation and its break-up process in this study area appeared to be controlled by the variations in SSC and bottom shear stress due to combined wave and current. The floc sizes showed less difference between the two sites under calm conditions. However, the near-bed *in situ* floc size in the aquaculture mudflat was 23% larger than that in the bare tidal flat in the severe erosion events, suggesting modulation of the flocculation process due to the extracellular polymeric substances (EPS) eroded from the seabed sediments at the aquaculture site, as the hydrodynamics were very similar between the two sites. A higher EPS content was observed in the sediment layer below the surface seabed at the aquaculture site. We conclude that abundant filter feeders alter floc properties and enhance flocculation by excretion of exopolymer particles.

Keywords: Tidal flat; Aquaculture; Suspended Sediment; Turbulence; Flocculation; Biological activities

1. Introduction

Flocculation of fine sediment particles has been widely observed in estuaries (Berhane et al., 1997; Guo et al., 2017; Van Leussen, 1988; Wang et al., 2013) and intertidal environments (Guo et al., 2018; Wells, 1989). Flocculation processes affect density, particle size, and settling velocity of suspended particles, which is crucially important for the sedimentation process and sediment transport (Dyer and Manning, 1999; Manning and Bass, 2006; Manning et al., 2006; Mikkelsen and Pejrup, 2001; Shao et al., 2011). Flocculation also plays an important role in biogeochemical cycles for nutrient (Maggi, 2009a), organic matter (Lee et al., 2019), and heavy metals (Biati et al., 2010; Karbassi et al., 2008) because of the adsorption ability and transport function of the particles in flocs. An enhanced settling velocity, caused by the combination of large flocs and high suspended sediment concentration, can lead to serious siltation (Guo et al., 2017). Considering the significant importance of the flocculation processes, it has been included in advanced numerical models of sediment transport (Engel and Schartau, 1999; Soulsby et al., 2013; Wang et al., 2013). Great attention has been paid to the hydrodynamic factors (Guo et al., 2017; Mhashhash et al., 2018; Schwarz et al., 2017), biological activity (Deng et al., 2019; Fettweis and Lee, 2017), and electrochemical processes (Karbassi et al., 2014) that affect fine sediment flocculation in estuaries and tidal flats.

Generally, flocculation can be formed by particle collision due to three fundamental factors: Brownian motion, fluid shear, and differential settling (Eisma, 1986; Tsai et al., 1987).

Brownian motion plays an important role at the beginning of the flocculation process with very fine primary particles when the turbulence is weak (Eisma, 1986; McCave, 1984; Partheniades and Emmanuel, 1993; Van Leussen, 1994). The effect of differential settling on the aggregation process is relatively greater in weak turbulence regions, for example, still water in laboratory experiments (Wendling et al., 2015) and estuarine and coastal environments during slack waters (Christie et al., 1999; Guo et al., 2017; Guo et al., 2018; Milligan et al., 2007). Of these three principle particle collision mechanisms, fluid shear is the dominant mechanism that drives particle collision in energetic flows (Liu et al., 2019; Manning, 2004; McAnally William and Mehta Ashish, 2000). Other factors can also influence the particle collision, such as suspended sediment concentration (SSC) (Manning, 2004; Mhashhash et al., 2018; Razaz et al., 2015; Tran et al., 2018; Van der Lee, 2000). The majority of researchers have paid more attention to the effects of turbulence and SSC in high turbulence regions.

Flocculation and floc break-up dynamics are influenced by physical hydrodynamic forces, electrochemical and biological processes (Wang et al., 2013). Important factors include salinity (Dobereiner and McManus, 1983; Gibbs and Konwar, 1986), suspended sediment concentration (Li et al., 1993; Razaz et al., 2015), turbulence (Guo et al., 2017; Winterwerp, 1998; Wolanski et al., 1992), and biological processes (Maggi, 2009b). In particular, biological processes can have a great effect on the size and stability of flocculated aggregates, by bonding suspended particles and organic matters together (Engel and Schartau, 1999; Heinonen et al., 2007; Wang et al., 2013).

Some research suggests that biological processes, e.g., algae growth and organic gelling, play an integral role in the dynamic process of flocculation (Wotton, 2004, 2005). At present, several types of plankton are recognized as a source of extracellular exopolymer particles (EPS) (Passow, 1994; Passow, 2000; Passow, 2002a, 2002b). Because of their high stickiness, the ubiquitous and abundant gel-particles enhance the aggregation of solid, non-sticky suspended sediment particles (Chen et al., 2005; Droppo, 2001; Lee et al., 2012; Passow, 2002b). Eisma (1986) proposed that bacteria, algae, and higher plants participate in floc formation through the release of mucopolysaccharides, which glue the fine sediment particles together. Experimental study results indicated that extracellular polymeric substances can increase the floc size by as much as one order of magnitude (Tan et al., 2012).

Both laboratory and field experiments have confirmed that some species of suspension feeder contribute to the presence of polymeric substances in marine ecosystems, due to the mucus, acidic and mixed mucopolysaccharides secreted by benthic suspension feeders (Heinonen et al., 2007; Li et al., 2008; McKee et al., 2005). For example, Li et al. (2008) suggested that large aggregates formed in direct relation to the number of polymeric substances produced by blue mussels *Mytilus edulis* and sea vases *Ciona intestinalis* under laboratory conditions. Heinonen et al. (2007) also confirmed through both laboratory experiments and field measurements that several benthic suspension feeders, including blue mussels and bay scallops, could facilitate the flocculation of organic matter and particles by producing polymeric substances.

Due to the complexity of biological processes and the fact that they are not easy to control or analyze in the laboratory (Dyer and Manning, 1999), the mechanism and importance of biological activity in flocculation dynamics are not clear yet. Furthermore, the influence of biological activity in coastal waters is even more difficult to quantify. For example, the floc sizes of suspended particles usually change continuously under natural conditions, because the flocculation process actually remains in a nonequilibrium state due to the influence of the dynamic changes of currents, waves, SSC, and the biological factors (Dyer and Manning, 1999; Guo et al., 2018). A better understanding of flocculation dynamics with and without biological modulation is needed.

This paper presents the temporal variation of in-situ floc size between two study sites (one a bare tidal flat and the other a clam aquaculture zone), which shared almost the same physical conditions but had distinctly different biological conditions. The objective is to examine the difference and resemblance of flocculation and floc break-up dynamics between the bare tidal flat and the flat subject to biological activities and to discuss the influence of biological processes on flocculation.

2. Background

The study area is situated at Rudong intertidal flat on the Jiangsu coast, eastern China. The intertidal flat on the central Jiangsu coast faces the South Yellow Sea, with a maximum width of 7–10 km (Ren, 1986) and a mean slope of 0.09% (Chen et al., 2010). The well-known radial sand ridge system acts as the main source of sediment in the coastal zone due to erosion in the offshore region and longshore transport (Du et al., 2019; Wang et al., 2012; Wang et al., 2004; Xing et al., 2012). The bottom sediment in the mid-intertidal zone at Rudong is composed of silty sand and sandy silt (Wang et al., 2012).

The Rudong Coast is characterized by a macro-tidal hydrodynamic setting, which is dominated by regularly semidiurnal tides, with a mean tidal range of 4.61 m and an extreme tidal range exceeding 8.0 m (Zhao and Gao, 2015).

The two sites (Site S1 and S2, Fig. 1) are located on the intertidal flats of the Rudong coast. Site S1 was on an aquaculture farm and Site S2 was on the undisturbed intertidal flat, with a distance of 1.4 km between the two sites. The activities of the suspension-feeding bivalve *M. meretrix* clams at Site S1 include burrowing, locomotion, suspension-feeding, pelletization, and excreting pseudo-fecal pellets (Gosling, 2015). The clams usually bury themselves at depths of 5 to 10 cm (Lee et al., 2007), and emerge to feed during periods of inundation. Mucus-like substances released by mucopolysaccharides mucocytes of filter feeders, which play a key role in particle transport and different ecological functions for bivalves, could contribute to the EPS (Gosling, 2015; Passow, 2002b; Wotton, 2005). The concentration of EPS varies in different marine settings and peaks at the location inhabited by dense assemblages of filter feeders (Li et al., 2008).

3. Methods

3.1. In situ measurements

From 24 August to 28 August 2016, two observation sites were established 1.5 km away from the seawall (Fig.1). We measured the floc size and other physical parameters including salinity, temperature, wave, current, the grain size of sea-bed sediment, to determine the similarity of the physical conditions between the two sites.

In situ measurements were started synchronously for all instruments at both sites before submersion and were left in place over nine consecutive tidal cycles at both sites. An acoustic Doppler velocimeter (ADV, 6MHz, Nortek AS.; measurement accuracy: ±1 mm/s; sampling rate: 16 Hz; sampling at 16 Hz for 256 sec every 5 min), a self-logging turbidity–temperature sensor (OBS-3A, Campbell Scientific, Inc., USA; sampling interval: 2.5 min), a wave–tide recorder (SBE26 plus SEAGAUGE, Sea-Bird Electronics Inc., USA; Measured accuracy: 0.01% of the fullscale; sampling interval: 10 minutes) and a LISST particle sizer (manufacturer: Sequoia Scientific, Inc.; Type: C; size-range: 2.5-500 microns) were deployed at each observation site.

Nortek vector current meters were deployed down-looking with the transmit transducer at a height of 0.37 m above the sea bed and were used to measure 3D velocity at 16 Hz (4096 points per 5 min time-series). The distance from the transmit transducer to the surface of the sea bed was also recorded to measure the changes of the sea bed due to erosion or accretion. The increasing values of distance from the probe to bed denote erosion, and decreasing values denote accretion.

The OBS-sensors were situated 0.16 m above the sea bed to measure turbidity, salinity, and water temperature every 150 seconds. In order to measure the primary particle size distribution of suspended sediments, water samples were collected within the bottom boundary layer of the water column (0.2 m above the seabed) with a water sampler on boats near two sites, whilst the instruments were submerged from August 24 to August 28. The water samples were also used to calibrate the turbidity values recorded by OBS-3A in the laboratory.

The wave and tide recorders were deployed horizontally on the sea bed, with the pressure sensors situated 0.1m above the sediment surface, monitoring pressure for 256 seconds at 4 Hz with a 10 minutes burst interval.

Particle size distribution was observed with the laser in-situ scattering and transmissometry instrument (LISST–100X with 90% path reduction module) continuously with a sampling interval of 2 minutes at 0.15 m above the sea bed at both observation sites. Whilst the bed was exposed, three surface sediment samples (0-5 cm) were collected to measure the organic matter content, which was determined by loss on ignition (LOI) after combustion. In addition, surficial sediment samples were collected from the uppermost 2 cm for grain size analysis (using Mastersizer 2000 laser diffraction particle size analyzer), and this sampling work conducted during August 24 and August 28. To estimate the population density of clams, three sediment samples of 0.3 m × 0.3 m × 0.1 m were collected from the tidal flat at each site and then sifted through a 1-mm mesh sieve. To measure the extracellular polymeric substances (EPS) content of bottom sediment, three sediment cores (each core has a diameter of 0.08 m and a depth of 0.30 m) were also collected at each site on 20 September 2018.

3.2. Sample analysis and data processing

Turbidity (T, measured in nephelometric turbidity units, NTU) derived from the optical techniques, can be used to accurately estimate suspended sediment concentration (SSC; unit: $g\ L^{-1}$) in the bottom boundary layer after calibrating the turbidity measurements with in situ collected water samples (Downing, 2004). The linear relationships established via calibration between the turbidity T (NTU) and in situ SSC ($g\ L^{-1}$) were expressed as follows:

$$SSC = 0.0033 \times T - 0.0734 \qquad (1)$$

R=0.913, N=18, 0.16 m above the seabed at Site S1.

$$SSC = 0.0101 \times T + 0.0055 \qquad (2)$$

R= 0.996, N= 12, 0.16 m above the seabed at Site S2.

where R is the correlation coefficient for the fitted relationship, and N is the number of data pairs used for the regression analysis (Fig. 2).

Water depth, significant wave height, and significant wave period were calculated using the program package provided by the manufacturer. The raw data derived from LISST were converted to volume concentration distribution (32 classes, logarithmically spaced between 2.5 and 500 μm) according to the manufacturer's manual based on scattering from spherical particles. According to the suggestions in the LISST-100X manual, the data were disregarded when transmission values were < 0.10. Mean floc sizes (D_M) of the sediment in suspension were then estimated from the volumetric size distributions. In data processing, care must be taken when there were raised tails at the ends of the distribution curves (the last 2 classes). These tails may be an artifact or caused by the particles greater than the instrument range of 500 μm for Lisst-100X type-C (Gartner et al., 2001). According to Mikkelsen et al. (2005), we checked the original data of LISST-100X and re-computed the D50 after deleting the 2 largest size classes (390 μm & 460 μm) in this study.

The primary particle size distribution of bottom sediment samples and in situ water samples were measured using Mastersizer 2000 granulometer after ultrasonic shaking for 2 min (Malvern Instruments Ltd.; measuring range 0.02–2,000 μm; reproducibility error <3%). Before the test, the bottom sediment samples were soaked in 30 g L^{-1} $Na_6O_{18}P_6$ solution for 24 h in order to remove organic matter and deflocculate potential aggregates.

The EPS contents of different layers (0~0.2 cm, 0.2~0.5 cm, 0.5~1 cm, 1~2 cm, 2~3 cm, 3~4 cm, 4~5 cm, 5~7 cm, and 7~9 cm depth below the surface seabed) in sediment cores were extracted according to the method modified from Orvain et al. (2014) and Chen et al. (2017a). EPS was extracted from approximately 5 mL of fresh sediment and placed in 50 mL centrifugation tubes in 25 mL of 0.2 μm filtered and sterilized artificial seawater (ASW). After 1 h of incubation in ASW, the sediment was added with ~1 g of cation exchange resin (CER, Na+). After resuspension, tubes were gently agitated (4 °C, 500 rpm, 60 min) in the dark. The residual solids in the supernatant were removed by high-speed centrifugation (10,000g) for 15 min. Total EPS was collected in the supernatant after filtering through a 0.45 μm filter membrane and kept frozen (−20 °C) for further analysis. The EPS yields were represented as polysaccharides. The anthrone carbohydrate method, as proposed by Raunkjær et al. (1994), was applied for the measurement of polysaccharide content in EPS with glucose as the standard.

3.3. Shear rate

The horizontal velocity (u, v) and vertical velocity (w) measured by ADV can be broken up into mean, wave, and turbulent components (Bian et al., 2018). For example, $u(t)$ can be expressed as $u = \bar{u} + \tilde{u} + u'$, where $\bar{u}$ is the burst-averaged velocity, $\tilde{u}$ is the orbital wave velocity, and u' is the turbulent fluctuation. An energy spectrum analysis with simple moving-average filter procedure, as outlined in Williams et al. (2003), was used to remove the wave-induced fluid motion waves (Soulsby and Humphery, 1990).

The bed shear stress (τ_c) is linearly related to the turbulent kinetic energy within the constant stress layer (Soulsby and Dyer, 1981):

$$\tau_c = \rho_w {u_*}^2 = C\rho_w \frac{\overline{u'^2}+\overline{v'^2}+\overline{w'^2}}{2} \tag{3}$$

in which the value of coefficient C is set to 0.19 (Kim et al., 2000; Pope et al., 2006), and ρ_w is the density of seawater, u_* is the friction velocity (Whitehouse et al., 2000).

The bed shear stress due to waves (τ_w) was obtained as a function of the wave orbital velocity U_w and the friction factor f_w (Fredsoe and Deigaard, 1992; Soulsby, 1997):

$$\tau_w = \frac{1}{2}\rho f_w \mathrm{U}_w^2 \tag{4}$$

in which the wave friction factor f_w depend on the hydraulic regime and can be expressed as (Soulsby, 1997).

$$f_w = \begin{cases} 2R_w^{-0.5}, & R_w \leq 5\times 10^5\ (laminar) \\ 0.0521R_w^{-0.187}, & R_w > 5\times 10^5\ (smooth\ turbulent) \\ 0.237r^{-0.52}, & (rough\ turbulent) \end{cases} \tag{5}$$

where $R_w\ (= U_w A/v)$ is the wave Reynolds number, $r\ (= A/k_s)$ is the relative roughness. A ($=U_w T/2\pi$) is the semi-orbital excursion, T is the wave period and $k_s\ (= 2.5d_{50})$ is Nikuradse roughness, d_{50} is the median grain size of the seabed sediment as recommended by Soulsby (1997).

The wave orbital velocity (U_w) is estimated by linear wave theory:

$$U_w = \frac{\pi H_s}{T sinh(kh)} \quad (6)$$

where H_s is the wave height (m) obtained from wave–tide recorder, k ($= 2\pi/L$, $L = (gT^2/2\pi)\tanh(kh)$) is the wavenumber, h is water depth (m) measured by wave–tide recorder, g is the gravitational acceleration (9.8 m^2 s^{-1}), and T is the wave period.

The total bed shear stress due to waves and currents (τ_{cw} and τ_{cw_max}, measured in N m^{-2}) is the combined stress due to currents (τ_c) and to waves (τ_w) based on the model of Soulsby (1997):

$$\tau_{cw} = \tau_c \left[1 + 1.2\left(\frac{\tau_w}{\tau_c+\tau_w}\right)^{3.2}\right] \quad (7)$$

$$\tau_{cw\_max} = [(\tau_{cw} + \tau_w \cos\varphi)^2 + (\tau_w \sin\varphi)^2]^{0.5} \quad (8)$$

where φ is the angle between current direction and direction of wave travel.

To quantify the effect of turbulence on floc creation and break-up, we calculated the shear rate *G* following (Pejrup and Mikkelsen, 2010):

$$G = \sqrt{\frac{u_*^3(1-{}^{z}/_{h})}{\upsilon \kappa z}} \quad (9)$$

where G represents the shear rate (s^{-1}), which is usually used as a proxy of the turbulence imposed on floc creation (Dyer and Manning, 1999; Leussen, 1994; Schwarz et al., 2017; Wang et al., 2013); υ is the temperature corrected kinematic viscosity of seawater (m^2 s^{-1}); κ is von Karman constant (0.41); z is the distance between the sampling volume and the sea bed.

3.4. Effective density

The effective density of the flocs ($\Delta\rho$, kg/m^3) defined as the difference between the particle and water densities, was calculated by (Fettweis, 2008):

$$\Delta\rho = \rho_f - \rho_w = (1 - \frac{\rho_w}{\rho_p}) \frac{SSC}{VC} \tag{10}$$

in which SSC was estimated from OBS-3A measurements (Eq. 1-2), VC is the volume concentration measured by LISST-100x, and the ρ_f is the floc density.

4. Results

We first compared the biological settings between the two sites and found differences in terms of biomass and EPS content. To determine the differences in the physical setting between the two monitoring sites, we compared several relevant parameters, including wave characteristics, tidal current, grain size, suspended sediment concentration, and the grain size of suspended sediments and bottom sediment. These parameters could affect the flocculation, and we show here that the physical settings were very similar between these two sites. There is no significant difference in salinity and temperature between tides and sites during the observation period, therefore we focus on the hydrodynamic characteristics and biological factors.

4.1. The density of *Meretrix and* EPS contents

There was a great difference in the clam density between the two sites. On 25 September 2016, the density of *Meretrix* was 137 $ind.m^{-2}$ and 3.7 $ind.m^{-2}$ for Site S1 and S2, respectively. On 20 September 2018, the density of *Meretrix* was 211 $ind.m^{-2}$ at Site S1, and there were no M. *Meretrix* found at Site S2. The values of organic content in the surface sediment at Site S1 (2.07%) were smaller than that at Site S2 (2.35%).

The variation of EPS content of the sediment with depth is shown in Fig. 3 for the two sites. At Site S1 the EPS concentration (represented by EPS total polysaccharides) ranged from 80.07 to 180.38 $\mu g\ g^{-1}$ DW, with a mean value of 138.95 $\mu g\ g^{-1}$ DW. For Site S2, the depth mean value was slightly lower, at 120.43 $\mu g\ g^{-1}$ DW, ranged from 79.02 to 248.47 $\mu g\ g^{-1}$ DW. Despite the similar vertical mean value, there was a noticeable difference between the two sites in layers deeper than 0.5 cm. The EPS content at Site S1 was about 47 % higher compared to Site S2 from 0.5 to 8 cm below the flat surface, which is inhabited by the clams. Whereas, the very surficial layer of Site S2 showed a much higher content.

According to Malarkey et al. (2015), the EPS contents ranged between 100~1000 $\mu g\ g^{-1}$ DW in sandy muds and sands with low mud content. In the laboratory experiments, the EPS contents ranged between 70 ~150 $\mu g\ g^{-1}$ DW in the sediment (108 μm, incubated with Bacillus subtilis for 5~22 d) sampled in Jiangsu province (Chen et al., 2017a), and the values are close to our study. In this study, the clams had a great influence on the sediment below the flat surface (layers deeper than 0.5 cm), however, the EPS contents were reduced due to the filter-feeding of clams.

In fact, EPS can be produced by a wide range of organisms, such as bacteria, diatoms, and macrofauna (Chen et al., 2017a; Heinonen et al., 2007; Passow, 2002b). The clams filter algae and destroy the biofilms which contain abundant EPS, therefore, the EPS content is not proportional to the clam density at Site S1.

The EPS, produced by the microbes and the algae, could be ingested or reabsorbed by the clams when filter-feeding (Gosling, 2015). In other words, the filter-feeding activities of clams could lead to a lower EPS content in the surface sediment, whereas the higher EPS below the surface may be a consequence of higher bioturbation at the site. A possible explanation of this could be due to the improvement of the permeability of soils due to bioturbation (from clam *M. meretrix* bio-activities), which also enabled the deeper penetration of oxygen, flow, and nutrients below the surface. As a result, a better environment inside the bed was provided for the enhancement of EPS production. In addition, amounts of mucus secreted by clam *M. meretrix* during their locomotion may also contribute to the EPS content.

4.2. Hydrodynamics, SSC, and seabed erosion/accretion

Significant wave heights (Hs) at Site S1 ranged from 0.04 to 1.30 m with an averaged value of 0.30 m, relatively smaller than wave heights at Site S2, which ranged from 0.03 to 1.31 m with a tidal-averaged value of 0.34 m. The values of τ_w showed similar trends with Hs and were greatly increased at both Sites during Tide T6-T9 due to the strong waves (Table 1).

As shown in Fig. 4a, the water levels are semi-diurnal at both sites. The current speeds varied between 0.06-0.39 m s^{-1} for Site S1 with the mean value of 0.23 m s^{-1}, and 0.09-0.39 m s^{-1} for Site S2 with the mean value of 0.24 m s^{-1}. The tidally-averaged values of current speeds were almost the same size at Site S1 and S2 during the observation period (Table 1), furthermore, the τ_c showed similar trends with the current speed at both sites (Fig. 4c and Fig. 4d). The values of τ_{cw_max} were smaller during tide T1-T5 and increased obviously with waves during tide T6-T9 at both sites (Table 1 and Fig. 4e).

Generally, the variations of SSCs for the two sites showed similar trends (Fig. 5c). Overall, the values of SSC increased with higher wave height and current velocity. At tide T2-T5, the SSCs observed at both sites had smaller values (Fig. 5c and Table 1). Whereas SSC values at both sites during T6, T8, and T9 increased by more than 50% with the largest wave height. As the wave and tidal current have been known to play a leading role in the sediment resuspension (Shi et al., 2017; Wang et al., 2006; Wang et al., 2012; Zhang et al., 2016), the higher SSCs during tides T6-T9 could be attributed to local resuspension caused by the stronger waves and horizontal advection which transport sediment from radial sand ridge system (Xing et al., 2012; Xiong et al., 2017).

The distance from the probe to bed measured by the ADV changed slightly from tide T1 to T4 (Fig. 5f). However, under the condition of strong wave actions, the bed level change showed general trends of erosion at the two sites during T5-T9 (Fig. 4 and Fig. 5f). During this event (T5-T9 in Fig. 5f) the net erosion over a tidal cycle was 22.4 mm, 24.7 mm, 12.9 mm, 13.5 mm, and 10.7 mm at Site S1, while the corresponding values for Site S2 were 15.1 mm, 16.9 mm, 2.8 mm, 10.6 mm and 2.6 mm.

4.3. Bottom and suspended sediment particle size

According to the grain size analysis of bottom sediment samples collected near the observation sites, the averaged mean size was 111.5 μm (3.2 Φ) and 139.7 μm (2.8 Φ) for Site S1 and S2, respectively. The bottom sediment was composed mainly of sands and silts. The sand contents were 90.09% and 97.21% for Site S1 and S2, while the silt contents were 9.08% and 2.79% for Site S1 and S2, respectively. Clay contents were low at both sites, accounting for 0.83% and 0% at Site S1 and S2, respectively.

The mean sizes of sediment in water samples collected near the bottom (0.20 m above the seabed) varied between 9-24 μm with an average value of 14 μm at Site S1, which was close to values of 11 - 27 μm and 17 μm for Site S2. The particle size distribution showed a unimodal distribution type (Fig. 6a and Fig. 6b).

4.4. Characteristics of the flocs

4.4.1. *In situ* mean particle size

The in situ mean size (D_M) is presented in Fig. 5b. The values of D_M were 70.81 ± 20.87 μm, 63.15 ± 20.29 μm for Site S1 and S2, respectively. In general, the change of D_M showed similar trends for both sites during the observation period (Fig. 5b). The tidally-averaged D_M for Site S1 was 11% larger than that for Site S2 (Fig. 5b and Table 1). Furthermore, the particle size distributions (PSD) for Site S1 showed the bimodal distribution with the peaks at 60 μm and 200-300 μm from T1 to T6 as a whole (Fig. 6c and Fig. 7). As shown in Fig. 6 and Fig. 7, micro-flocs or smaller flocs (Eisma, 1986) (<125 μm) were observed at both sites.

From T1 to T4, when the G reached its minimum during high water, the SSC increased obviously (03:10 in T1; 15:10 in T2; 03:40 in T3; 16:10 in T4). The increased SSC with low G was due in large part to the settling of suspended particles from the upper water column because the sediment observed by Lisst-100x and OBS sensors (situated near the seabed) was closed to the seabed. Moreover, at the same time, the floc size began to decrease with the high SSC (Fig. 5a~Fig. 5d).

Interestingly, the D_M showed a clear difference between Site S1 and S2 during tide T7-T9 (Fig. 5b; Fig. 6c-d). The D_M at Site S1 was 23% larger than those at Site S2, with the values of 59 μm, 47 μm, 39 μm at Site S2 for tide T7, T8 and T9, respectively. In contrast, the corresponding values of Site S1 were 69 μm, 58 μm and 49 μm during the same periods, respectively (Table 1). Moreover, the values of D_M varied significantly during different tides at two sites, whereas floc sizes at Site S2 showed weaker variations compared with Site S1 during tide T7-T9. As shown in Fig. 5b, within a tidal cycle during erosion events (T5-T9), D_M peaked during the initial flood in each tidal period and remained considerably higher until mid-flood. During the high water level, the mean sizes began to decrease and subsequently reached the minimum values at the mid-ebb stage of the tide when the SSCs peaked.

In situ PSD of in-situ suspended particles showed great differences between the two sites during T7-T9 (Fig. 6e, Fig. 6f, and Fig. 7). At Site S1, the PSD implied that in situ suspended sediments were composed of micro flocs (<128 μm) and macroflocs (>128 μm), while the suspended sediments at Site S2 were mostly made up of microflocs and the frequency of occurrence of a coarser fraction reduced (Fig. 6e and Fig. 6f). At both sites, there was a peak in floc sizes that was just greater than 100 μm during the flood and high water periods. During the ebb, this peak was reduced, and the component of particles with diameter < 50 μm increased around the time of mid-ebb at both sites; at the same time, the proportion of particles with diameter > 50 μm declined dramatically (the blue line in Fig. 6e and Fig. 6f) as the SSC peaked (Fig. 5c). Both sites showed a greater abundance of small flocs during the ebb tide and the primary particles populations increased significantly. This phenomenon indicates an intense floc break-up process that accompanied the peak in SSC.

4.4.2. Effective density

The values of $\Delta\rho$ were 384 kg m^{-3} (between 58-681 kg m^{-3}), 429 kg m^{-3} (between 34-1313 kg m^{-3}) for Site S1 and S2, respectively. The $\Delta\rho$ decreased with the increasing D_M and appeared to be negatively correlated with the mean size of flocs for the two sites (Fig. 8), which is consistent with other studies (Guo et al., 2017; Wang et al., 2013). The mass fractal dimension (Nf) was determined as the relationship between $\Delta\rho$ and D_M ($\Delta\rho \propto (\rho_p - \rho_w)\left(\frac{D_M}{Dp}\right)^{Nf-3}$) (Fettweis, 2008; Hill et al., 1998; Kranenburg, 1994; Mikkelsen and Pejrup, 2001). In thisstudy, the values of estimated Nf ranged between 2.10-2.50 with the optimal fitting value of 2.30 for Site S1, and between 1.35-2.22 with the optimal fitting values of 1.85 for Site S2. Previous studies suggested that larger Nf related to strong flocs, while lower Nf related to fragile flocs (Dyer and Manning, 1999; Kranenburg, 1994; Winterwerp, 1998).

5. Discussion

5.1. Controlling factors on the flocculation/deflocculation

Many studies have focused on the effect of turbulent shear and SSC on the coagulation process (Guangquan et al., 2014; Guo et al., 2017; Guo et al., 2018; Tran et al., 2018). Some research found that the flocculation process was controlled by turbulence more than other factors (Schwarz et al., 2017; Wang et al., 2013). In this study, the pattern of temporal variation of D_M was contrary to variations of SSC at both sites, suggesting that SSCs had an important effect on the dynamic process of flocculation (Fig. 5b, c). The correlation between D_M and SSC, as shown in Fig. 9, D_M decreased with the increasing SSC, exhibiting a negative power-law relationship with the coefficient of determination (R^2) of 0.98, 0.79 for Site S1 and S2, respectively (Fig. *10*a and 10b). The relationships between D_M and SSC can be represented as follows:

$$D_{M\_S1} = 36\,SSC^{-0.43} \quad (11)$$

$$D_{M\_S2} = 41\,SSC^{-0.32} \quad (12)$$

The SSC appeared to be a significant factor in flocculation and the floc break-up processes, which agrees with the findings of Dyer and Manning (1999), Guo et al. (2017), and Burban et al. (1989). According to Guo et al. (2017), when G became larger than 3 s^{-1}, D_M decreased with the increasing G, and the floc size showed a negative relationship with SSC during tidal periods except for water slack periods when deposition of flocs in the water column occurred.

However, the correlation between D_M and shear rate G_{u*} calculated using u* exhibited a wide scatter and had weaker correlations for both sites (Fig. 10c and 10d). This result indicates that the shear rate induced by current had a smaller effect on the variations of D_M compared to SSC.

Many studies have focused on the relationships between floc size, shear stress due to current, and shear rate (Ramírez-Mendoza et al., 2016; Schwarz et al., 2017; Wang et al., 2013). Considering the strong waves in natural environments, more studies are needed to determine the combination mechanism of waves and currents. In this study, the wave heights increased and led to sediment resuspension and high values of SSC during T5 to T9. The flocculation processes were also mediated through direct and indirect influences of the waves. Ramírez-Mendoza et al. (2016) suggested that using the effective kinetic energy due to combined currents and waves can improve the prediction of flocculation when compared to estimates based on shear stress due to currents. In this study, the wave-current shear rate, G_{CW}^{-m}, was used to consider the effect of combined waves and currents.

We estimated the G_{CW} using τ_{cw} as defined by equations (3), (7), and (9). This significantly improved the correlation between the shear rate G_{CW} and D_M with the R^2 increasing from 0.41 to 0.87 for Site S1 (Fig. 10c and 10e), and from 0.47 to 0.77 for Site S2 (Fig. 10d and 10f). This improvement highlights how waves also play an important role in sediment flocculation, suggesting that the combined wave-current shear stress should be used when waves are present. The D_M is proportional to G_{u*}^{-m}, or G_{CW}^{-m}, with the exponent m ranging between 1.2 and 1.6, and this trend is similar to previous studies by Manning and Dyer (1999) and Wang et al. (2013). In the study by Wang et al. (2013), the correlation with D_M is significantly improved from -0.59 to -0.83 by replacing the G with SSC·G. In this study, when G_{CW} is replaced by $SSC \cdot G_{CW}$, the correlation with D_M is also improved with R^2 being increased from 0.87 to 0.99 for Site S1 (Fig. 10e and 10g), and from 0.77 to 0.80 for Site S2 (Fig. 10f and 10h), using the following formula (Fig. 10g and 10h):

$$D_{M\_S1} = 64\,(SSC \cdot G_{CW})^{-0.35} \qquad (13)$$

$$D_{M\_S2} = 63\,(SSC \cdot G_{CW})^{-0.27} \qquad (14)$$

The improved correlation between D_M and $SSC \cdot G_{CW}$ indicates that D_M decreases with turbulence induced by combined waves and currents and increasing SSC. The SSC is positively correlated to τ_{cw_max} with the R^2 of 0.86 and 0.78 for S1, and S2, respectively (Fig. 11), indicating that the SSC is dominated largely by local resuspension induced by turbulence. Therefore, the variation of D_M is mainly controlled by the G_{CW} and the local resuspended SSC.

Several studies reported that flocs were broken up by the turbulent shear when G was small under natural conditions (Guo et al., 2017; Markussen and Andersen, 2014). For example, according to Guo et al. (2017), a plateau of D_M for G values < 3 s^{-1} was identified, and when the G became larger than 3 s^{-1}, D_M decreased significantly; Furthermore, the floc size showed a negative relationship with SSC during tidal periods, except for slack-water periods, when deposition of flocs occurred (section 4.2.2 and Fig.7 in Guo et al. (2017)). As mentioned by Dyer and Manning (1999), when the dissipation rates ranged between 2.77 -277 s^{-1} in their laboratory experiments, the proportion of large flocs declined with increasing SSC, presumably attributed to the disruption caused by particle collisions. Some of the experiments in their study were conducted with the G < 10 s^{-1} (section 3.1 and Fig.3 in Dyer and Manning (1999)). In the study by Wang et al. (2013), the floc size decreases both with concentration and turbulence, and again G was small ranging between 0 and 14 s^{-1}. In the study by Markussen and Andersen (2014), the flocs are broken up by the turbulence when the shear rate is in the range of $4 - 12\ s^{-1}$, and the D_M remains constant when the G is larger than 12 s^{-1}. Hence the assertion that the flocs were broken up by relatively low levels of turbulent shear is consistent with the findings of others.

5.2. Biological activities on the flocculation

Previous laboratory experiments have shown that bacterial biofilms are generally a thin surface layer that shears away within a very short space of time (e.g. < 10 seconds)(Chen et al., 2017a;

Chen et al., 2017b). When the bio-sedimentary matrix is eroded during disturbance events (i.e., high shear stress during spring tides, storms), EPS may support aggregation and change the floc characteristics of the entrained material (Chen et al., 2019; Heinonen et al., 2007; Li et al., 2008).

On account of the abundant quantity of clams on the tidal-flat at Site S1, the flocculation processes could be influenced by the following factors:

- The feces or pseudofaeces are produced or released by filter-feeding species (Biggs and Howell, 1984).
- The gathering of organic matter and plankton due to the filter-feeding process (Heinonen et al., 2007; Passow, 2002b), which promotes floc formation.
- The stickiness of extracellular polymeric substances (Lee et al., 2012), which increases the flocs size and breakage-resistance. Furthermore, because of the stickiness of the EPS, the bottom sediments "stick" together due to the EPS produced by clams (Chen et al., 2017a; Chen et al., 2017b; Heinonen et al., 2007; Passow, 2002b).

According to research from Kraeuter and Haven (1970), the size of pellets voided by the clam *Mercenaria mercenaria* ranges between 560-4750 μm (length range), which were out of the scope of the particle size range of the LISST-100X. Furthermore, the D_M and PSD for the 2 sites had similar values under calm conditions (T1-T4) and showed differences after severe erosion of seabed (Fig. 5). These phenomena indicate that the characteristics of flocs are not attributable to the feeding activity of clams directly.

At Site S1, when the tide came up the tidal flats, the clams secreted significant amounts of mucus during locomotion and feeding, which increased EPS content (Passarelli et al., 2014). Under more energetic conditions due to waves, the sea bed was eroded and the bottom sediments were rapidly resuspended due to the strong waves. According to previous studies, the EPS content in seawater is orders of magnitude lower than that in bottom sediments (Heinonen et al., 2007; Passow, 2002b). For instance, Heinonen et al. (2007) obtained an EPS content of 0.12 μg g^{-1} DW in seawater. The peak concentrations of EPS in seawater are generally around 1 μg g^{-1} DW, far below the EPS content in sediment (Passow, 2002b). Thus, the sub-surface sediments with higher EPS content were exposed and then resuspended in the water column under extreme events, which favored the increase of EPS content in the water. On the basis that Site S1 suffered severe erosion of 17 mm from T5 to T9, the EPS released to water volume is estimated to be 1621 μg per square centimeter of seabed, based on an assumption that the seabed began to erode during T5 (Fig. 3b). By comparison, the EPS released to the water volume from Site S2, during the same period, would be 698 μg per square centimeter (Fig. 3b). This suggests that the seabed at Site S1 could have released 2 times more EPS than Site S2. The EPS content of the water at Site S1 increased by about 2 μg g^{-1} DW based on the average water depth of 1.60 m. As a result, the higher content of EPS in the bottom sediments, related to clam activities, released more EPS, which enhanced the density and resistance of flocs compared to the bare tidal flat.

During the severe erosion, the sub-surface sediments, which consist of EPS and EPS-enveloped particles, resuspended into the water column. The primary particles included in EPS-wrapped particles and EPS-supported flocs have stronger binding forces (Chen et al., 2017a; Passow, 2002b). Therefore, the mean size of flocs at Site S1 was larger than that at Site S2 during the storm. In contrast, the flocs at Site S2 were more fragile, and contain more primary particles.

As shown in Fig. 8, the larger Nf at Site S1 (2.30) may indicate that flocs were compact and stronger, in contrast to the fragile flocs at Site S2 with smaller Nf (1.85). This suggests that the biological activity plays a role in the flocculation process by modulating the density of flocs or enhancing the resistance of flocs against shear stress and break-up, which causes the differences in grain size and PSD of suspended sediments under extreme events (e.g. strong waves and severe bed erosion during T5-T9). This mechanism is different from the aggregation of diatom blooms related to sticky EPS, which directly participate in the flocculation process by gluing small particles together (Passow et al., 1994). It is worth mentioning that though $\Delta\rho$ is negatively correlated with D_M, the $\Delta\rho$ was decreased with the smaller D_M from T7 to T9; the estimating of $\Delta\rho$ based on SSC and VC may cause a deviation between theoretical calculations and real results for the density of suspended sediment; the OBS sensor is not usually sensitive to the sand (Bass et al., 2007), and the SSC may be underestimated in severe erosion event when seabed sediments were re-suspended; hence, the $\Delta\rho$ may also be underestimated. However, the $\Delta\rho$ was still negatively correlated with the D_M (Fig. *8*), in other words, the variation trend between $\Delta\rho$ and D_M was consistent with previous studies.

To some degree, these biological processes could explain the phenomena that flocs at Site S1 generally had a greater size in the severe erosion event and that the component of macro flocs was higher for the entire tidal period when compared to Site S2. The implication is that sedimentation and sediment transport will differ at the two sites because the EPS released by the clams at Site S1 has resulted in a change in floc properties and settling velocity. In other words, human activities, such as aquaculture, can change the sediment aggregation on the tidal-flats and thus may play a role in the sediment dynamics and transport rates. However, more quantitative studies are needed in order to evaluate the production of organic matter and extracellular EPS related to clams, to clarify the extent to which floc size and density are modulated by EPS concentration and the role of different types of biota in enhancing particulate flocculation in tidal environments.

6. Conclusions

This study analyzed flocculation dynamics at two physically similar but biologically different monitoring sites on the macro-tidal flat based on systematic field measurements. Our analysis demonstrates that the different responses of *in situ* floc size to changing SSC, turbulence, and flocculation processes could be attributed to the different biological conditions. For the site located in the clam aquaculture region (Site S1), the mean floc size, and the proportion of macro flocs components were larger than at the nearby bare tidal flat site (Site S2) during erosion event.

With increasing SSC, a marked decrease in mean floc size was observed. The shear rate G can affect the flocculation process by enhancing SSC. These results, taken together, confirm that the variation of suspended particle concentration and turbulence plays an important role in governing the floc aggregation and break-up processes on tidal flats. Meanwhile, the abundant suspension feeders (i.e., clam *M. meretrix*) are believed to influence floc formation, the stability of flocs, and floc size, through the sticky organic matter related to biological activities. Due to the ubiquitous and abundant nature of extracellular polymeric substances, the influence of biological processes on flocculation should receive greater attention in cohesive sediment studies.

Acknowledgments

The study is funded by the National Natural Science Foundation of China (41625021, 42076170). The authors thank Jieping Tang, Dezhi Chen, Yuan Li, and Haohao Lu who participated in the fieldwork and lab analysis. We also deeply appreciate the two reviewers who give constructive suggestions for the revision of the manuscript.

Literature Cited

Bass, S.J., McCave, I.N., Rees, J.M., Vincent, C.E., 2007. Sand and mud flux estimates using acoustic and optical backscatter sensors: measurements seaward of the Wash, southern North Sea. Geological Society, London, Special Publications 274, 25.https://doi.org/10.1144/GSL.SP.2007.274.01.04.

Berhane, I., Sternberg, R.W., Kineke, G.C., Milligan, T.G., Kranck, K., 1997. The variability of suspended aggregates on the Amazon Continental Shelf. Continental Shelf Research 17, 267-285.http://dx.doi.org/10.1016/S0278-4343(96)00033-7.

Bian, C.W., Liu, Z.Y., Huang, Y.X., Zhao, L., Jiang, W.S., 2018. On Estimating Turbulent Reynolds Stress in Wavy Aquatic Environment. Journal of Geophysical Research: Oceans 123, 3060- 3071.https://doi.org/10.1002/2017JC013230.

Biati, A., Karbassi, A.R., Hassani, A.H., Monavari, S.M., Moattar, F., 2010. Role of metal species in flocculation rate during estuarine mixing. International Journal of Environmental Science & Technology 7, 327-336.https://doi.org/10.1007/BF03326142.

Biggs, R.B., Howell, B.A., 1984. The estuary as a sediment trap: Alternate approaches to estimating its filtering efficiency, in: Kennedy, V.S. (Ed.), The Estuary As a Filter. Academic Press, pp. 107-129.

Burban, P.-Y., Lick, W., Lick, J., 1989. The flocculation of fine-grained sediments in estuarine waters. Journal of Geophysical Research: Oceans 94, 8323-8330.https://doi.org/10.1029/JC094iC06p08323.

Chen, J., Wang, Y.G., Cai, H., 2010. Profile characteristics study of the Jiangsu coast. Ocean Engineering 28, 90-96.https://doi.org/10.16483/j.issn.1005-9865.2010.04.009.

Chen, M.S., Wartel, S., Temmerman, S., 2005. Seasonal variation of floc characteristics on tidal flats, the Scheldt estuary. Hydrobiologia 540, 181-195.https://doi.org/10.1007/s10750-004-7143-6.

Chen, X.D., Zhang, C.K., Paterson, D.M., Thompson, C.E.L., Townend, I.H., Gong, Z., Zhou, Z., Feng, Q., 2017a. Hindered erosion: The biological mediation of noncohesive sediment behavior. Water Resources Research 53, 4787-4801.https://doi.org/10.1002/2016WR020105.

Chen, X.D., Zhang, C.K., Paterson, D.M., Townend, I.H., Jin, C., Zhou, Z., Gong, Z., Feng, Q., 2019. The effect of cyclic variation of shear stress on non-cohesive sediment stabilisation by microbial biofilms: The role of “biofilm precursors”. Earth surface processes and landforms 44, 1471-1481.https://doi.org/10.1002/esp.4573.

Chen, X.D., Zhang, C.K., Zhou, Z., Gong, Z., Zhou, J.J., Tao, J.F., Paterson, D.M., Feng, Q., 2017b. Stabilizing Effects of Bacterial Biofilms: EPS Penetration and Redistribution of Bed Stability Down the Sediment Profile. Journal of Geophysical Research: Biogeosciences 122, 3113-3125.https://doi.org/10.1002/2017JG004050.

Christie, M.C., Dyer, K.R., Turner, P., 1999. Sediment Flux and Bed Level Measurements from a Macro Tidal Mudflat. Estuarine, Coastal and Shelf Science 49, 667-688.https://doi.org/10.1006/ecss.1999.0525.

Deng, Z., He, Q., Safar, Z., Chassagne, C., 2019. The role of algae in fine sediment flocculation: In-situ and laboratory measurements. Marine Geology 413, 71-84.https://doi.org/10.1016/j.margeo.2019.02.003.

Dobereiner, C., McManus, J., 1983. Turbidity Maximum Migration and Harbor Siltation in the Tay Estuary. Canadian Journal of Fisheries and Aquatic Sciences 40, 117-141.https://doi.org/10.1139/f83-275.

Downing, J., 2004. Turbidity Monitoring, in: DOWN, R.D., LEHR, J.H. (Eds.), Environmental Instrumentation and Analysis Handbook. John Wiley & Sons, Inc., Hoboken, pp. 511-546.

Droppo, I.G., 2001. Rethinking what constitutes suspended sediment. Hydrological Processes 15, 1551-1564.https://doi.org/10.1002/hyp.228.

Du, J., Shi, B., Li, J., Wang, Y.P., 2019. 3 - Muddy Coast Off Jiangsu, China: Physical, Ecological, and Anthropogenic Processes, in: Wang, X.H. (Ed.), Sediment Dynamics of Chinese Muddy Coasts and Estuaries. Academic Press, pp. 25-49.

Dyer, K.R., Manning, A.J., 1999. Observation of the size, settling velocity and effective density of flocs, and their fractal dimensions. Journal of Sea Research 41, 87-95.https://doi.org/10.1016/S1385-1101(98)00036-7.

Eisma, D., 1986. Flocculation and de-flocculation of suspended matter in estuaries. Netherlands Journal of Sea Research 20, 183-199.http://dx.doi.org/10.1016/0077-7579(86)90041-4.

Engel, A., Schartau, M., 1999. Influence of transparent expolymer particles (TEP) on sinking velocity of Nitzschia closterum aggregates. Marine Ecology Progress Series 182, 69-76.https://doi.org/10.3354/meps182069.

Fettweis, M., 2008. Uncertainty of excess density and settling velocity of mud flocs derived from in situ measurements. Estuarine, Coastal and Shelf Science 78, 426-436.https://doi.org/10.1016/j.ecss.2008.01.007.

Fettweis, M., Lee, J.B., 2017. Spatial and Seasonal Variation of Biomineral Suspended Particulate Matter Properties in High-Turbid Nearshore and Low-Turbid Offshore Zones. Water 9.https://doi.org/10.3390/w9090694.

Fredsoe, J., Deigaard, R., 1992. Mechanics of Coastal Sediment Transport. World Scientific, Singapore.

Gartner, J.W., Cheng, R.T., Wang, P.-F., Richter, K., 2001. Laboratory and field evaluations of the LISST-100 instrument for suspended particle size determinations. Marine Geology 175, 199-219.https://doi.org/10.1016/S0025-3227(01)00137-2.

Gibbs, R.J., Konwar, L., 1986. Coagulation and settling of Amazon River suspended sediment. Continental Shelf Research 6, 127-149.http://dx.doi.org/10.1016/0278-4343(86)90057-9.

Gosling, E., 2015. Marine Bivalve Molluscs, Second ed. Wiley-Blackwell, Chichester.

Guangquan, Q., Jinfeng, Z., Qinghe, Z., Jinlong, X., Bo, X., 2014. Experimental Investigation of the Influence of Turbulence on the Flocculation and Settling of Cohesive Sediment. Journal of Tianjin University(Science and Technology) 47, 811-816.http://dor.org/10.11784/tdxbz201303022.

Guo, C., He, Q., Guo, L., Winterwerp, J.C., 2017. A study of in-situ sediment flocculation in the turbidity maxima of the Yangtze Estuary. Estuarine, Coastal and Shelf Science 191, 1-9.https://doi.org/10.1016/j.ecss.2017.04.001.

Guo, C., He, Q., van Prooijen, B.C., Guo, L., Manning, A.J., Bass, S., 2018. Investigation of flocculation dynamics under changing hydrodynamic forcing on an intertidal mudflat. Marine Geology 395, 120-132.https://doi.org/10.1016/j.margeo.2017.10.001.

Heinonen, K.B., Ward, J.E., Holohan, B.A., 2007. Production of transparent exopolymer particles (TEP) by benthic suspension feeders in coastal systems. Journal of Experimental Marine Biology and Ecology 341, 184-195.https://doi.org/10.1016/j.jembe.2006.09.019.

Hill, P.S., Syvitski, J.P., Cowan, E.A., Powell, R.D., 1998. In situ observations of floc settling velocities in Glacier Bay, Alaska. Marine Geology 145, 85-94.http://dx.doi.org/10.1016/S0025-3227(97)00109-6.

Karbassi, A.R., Heidari, M., Vaezi, A.R., Samani, A.R.V., Fakhraee, M., Heidari, F., 2014. Effect of pH and salinity on flocculation process of heavy metals during mixing of Aras River water with Caspian Sea water. Environmental Earth Sciences 72, 457-465.https://doi.org/10.1007/s12665-013-2965-z.

Karbassi, A.R., Nouri, J., Mehrdadi, N., Ayaz, G.O., 2008. Flocculation of heavy metals during mixing of freshwater with Caspian Sea water. Environmental Geology 53, 1811-1816.https://doi.org/10.1007/s00254-007-0786-7.

Kim, S.-C., Friedrichs, C.T., Maa, J.P.-Y., Wright, L.D., 2000. Estimating Bottom Stress in Tidal Boundary Layer from Acoustic Doppler Velocimeter Data. Journal of Hydraulic

Engineering 126, 399-406.https://doi.org/10.1061/(ASCE)0733-9429(2000)126:6(399).

Kraeuter, J., Haven, D.S., 1970. Fecal pellets of common invertebrates of lower York River and lower Chesapeake Bay, Virginia. Chesapeake Science 11, 159-173.https://doi.org/10.2307/1351239.

Kranenburg, C., 1994. The Fractal Structure of Cohesive Sediment Aggregates. Estuarine, Coastal and Shelf Science 39, 451-460.https://doi.org/10.1006/ecss.1994.1075.

Lee, A.-C., Lin, Y.-H., Lin, C.-R., Lee, M.-C., Chen, Y.-P., 2007. Effects of components in seawater on the digging behavior of the hard clam (Meretrix lusoria). Aquaculture 272, 636-643.https://doi.org/10.1016/j.aquaculture.2007.06.013.

Lee, B.J., Fettweis, M., Toorman, E., Molz, F.J., 2012. Multimodality of a particle size distribution of cohesive suspended particulate matters in a coastal zone. Journal of Geophysical Research: Oceans 117, 1-17.https://doi.org/10.1029/2011JC007552.

Lee, B.J., Kim, J., Hur, J., Choi, I.H., Toorman, E.A., Fettweis, M., Choi, J.W., 2019. Seasonal Dynamics of Organic Matter Composition and Its Effects on Suspended Sediment Flocculation in River Water. Water Resources Research 55, 6968-6985.https://doi.org/10.1029/2018WR024486.

Leussen, W.v., 1994. Estuarine macroflocs and their role in fine-grained sediment transport = Macrovlokken en hun bijdrage aan de slibtransporten in estuaria. University of Utrecht, Utrecht, p. 494.

Li, B., Ward, J.E., Holohan, B.A., 2008. Transparent exopolymer particles (TEP) from marine suspension feeders enhance particle aggregation. Marine Ecology Progress 357, 67-77.https://doi.org/10.3354/meps07290.

Li, Y., Wolanski, E., Qinchun, X., 1993. Coagulation and Settling of Suspended Sediment in the Jiaojiang River Estuary, China. Journal Of Coastal Research 9, 390-402.

Liu, J., Liang, J.-H., Xu, K., Chen, Q., Ozdemir, C.E., 2019. Modeling Sediment Flocculation in Langmuir Turbulence. Journal of Geophysical Research: Oceans 124, 7883-7907.https://doi.org/10.1029/2019JC015197.

Maggi, F., 2009a. Biological flocculation of suspended particles in nutrient-rich aqueous ecosystems. Journal of Hydrology 376, 116-125.https://doi.org/10.1016/j.jhydrol.2009.07.040.

Maggi, F., 2009b. Biological flocculation of suspended particles in nutrient-rich aqueous ecosystems. Journal of Hydrology 376, 116-125.https://doi.org/10.1016/j.jhydrol.2009.07.040.

Malarkey, J., Baas, J.H., Hope, J.A., Aspden, R.J., Parsons, D.R., Peakall, J., Paterson, D.M., Schindler, R.J., Ye, L., Lichtman, I.D., Bass, S.J., Davies, A.G., Manning, A.J., Thorne, P.D., 2015. The pervasive role of biological cohesion in bedform development. Nature Communications 6, 6257.https://doi.org/10.1038/ncomms7257.

Manning, A.J., 2004. The Observed Effects of Turbulence on Estuarine Flocculation. Journal Of Coastal Research, 90-104.

Manning, A.J., Bass, S.J., 2006. Variability in cohesive sediment settling fluxes: Observations under different estuarine tidal conditions. Marine Geology 235, 177-192.http://dx.doi.org/10.1016/j.margeo.2006.10.013.

Manning, A.J., Bass, S.J., Dyer, K.R., 2006. Floc properties in the turbidity maximum of a mesotidal estuary during neap and spring tidal conditions. Marine Geology 235, 193-211.https://doi.org/10.1016/j.margeo.2006.10.014.

Manning, A.J., Dyer, K.R., 1999. A laboratory examination of floc characteristics with regard to turbulent shearing. Marine Geology 160, 147-170.http://dx.doi.org/10.1016/S0025-3227(99)00013-4.

Markussen, T.N., Andersen, T.J., 2014. Flocculation and floc break-up related to tidally induced turbulent shear in a low-turbidity, microtidal estuary. Journal of Sea Research 89, 1-11.http://dx.doi.org/10.1016/j.seares.2014.02.001.

McAnally William, H., Mehta Ashish, J., 2000. Aggregation Rate of Fine Sediment. Journal of Hydraulic Engineering 126, 883-892.https://doi.org/10.1061/(ASCE)0733-9429(2000)126:12(883).

McCave, I.N., 1984. Size spectra and aggregation of suspended particles in the deep ocean. Deep Sea Research Part A. Oceanographic Research Papers 31, 329-352.https://doi.org/10.1016/0198-0149(84)90088-8.

McKee, M.P., Ward, J.E., MacDonald, B.A., Holohan, B.A., 2005. Production of transparent exopolymer particles (TEP) by the eastern oyster Crassostrea virginica. Marine Ecology Progress Series 288, 141-149.https://doi.org/10.3354/meps288141.

Mhashhash, A., Bockelmann-Evans, B., Pan, S., 2018. Effect of hydrodynamics factors on sediment flocculation processes in estuaries. Journal of Soils and Sediments 18, 3094-3103.https://doi.org/10.1007/s11368-017-1837-7.

Mietta, F., Chassagne, C., Manning, A.J., Winterwerp, J.C., 2009. Influence of shear rate, organic matter content, pH and salinity on mud flocculation. Ocean Dynamics 59, 751-763.https://doi.org/10.1007/s10236-009-0231-4.

Mikkelsen, O., Pejrup, M., 2001. The use of a LISST-100 laser particle sizer for in-situ estimates of floc size, density and settling velocity. Geo-marine Letters 20, 187-195.https://doi.org/10.1007/s003670100064.

Mikkelsen, O.A., Hill, P.S., Milligan, T.G., Chant, R.J., 2005. In situ particle size distributions and volume concentrations from a LISST-100 laser particle sizer and a digital floc camera. Continental Shelf Research 25, 1959-1978.https://doi.org/10.1016/j.csr.2005.07.001.

Milligan, T.G., Hill, P.S., Law, B.A., 2007. Flocculation and the loss of sediment from the Po River plume. Continental Shelf Research 27, 309-321.https://doi.org/10.1016/j.csr.2006.11.008.

Orvain, F., De Crignis, M., Guizien, K., Lefebvre, S., Mallet, C., Takahashi, E., Dupuy, C., 2014. Tidal and seasonal effects on the short-term temporal patterns of bacteria, microphytobenthos and exopolymers in natural intertidal biofilms (Brouage, France). Journal of Sea Research 92, 6-18.https://doi.org/10.1016/j.seares.2014.02.018.

Partheniades, Emmanuel, 1993. Turbulence, Flocculation and Cohesive Sediment Dynamics. Nearshore & Estuarine Cohesive Sediment Transport 42, 40-59.https://doi.org/10.1029/CE042p0040.

Passarelli, C., Olivier, F., Paterson, D.M., Meziane, T., Hubas, C., 2014. Organisms as cooperative ecosystem engineers in intertidal flats. Journal of Sea Research 92, 92-101.https://doi.org/10.1016/j.seares.2013.07.010.

Passow, U., 1994. Distribution, size, and bacterial colonization of transparent exopolymer particles (TEP) in the ocean. Mar Ecol Prog Ser 113, 185-198.https://doi.org/10.3354/meps113185.

Passow, U., 2000. Formation of transparent exopolymer particles, TEP, from dissolved precursor material. Marine Ecology Progress Series 192, 1-11.https://doi.org/10.3354/meps192001.

Passow, U., 2002a. Production of transparent exopolymer particles (TEP) by phyto- and bacterioplankton. Marine Ecology Progress 236, 1-12.https://doi.org/10.3354/meps236001.

Passow, U., 2002b. Transparent exopolymer particles (TEP) in aquatic environments. Progress in Oceanography 55, 287-333.https://doi.org/10.1016/S0079-6611(02)00138-6.

Passow, U., Alldredge, A.L., Logan, B.E., 1994. The role of particulate carbohydrate exudates in the flocculation of diatom blooms. Deep Sea Research Part I: Oceanographic Research Papers 41, 335-357.https://doi.org/10.1016/0967-0637(94)90007-8.

Pejrup, M., Mikkelsen, O.A., 2010. Factors controlling the field settling velocity of cohesive sediment in estuaries. Estuarine, Coastal and Shelf Science 87, 177-185.http://dx.doi.org/10.1016/j.ecss.2009.09.028.

Pope, N.D., Widdows, J., Brinsley, M.D., 2006. Estimation of bed shear stress using the turbulent kinetic energy approach—A comparison of annular flume and field data. Continental Shelf Research 26, 959-970.https://doi.org/10.1016/j.csr.2006.02.010.

Ramírez-Mendoza, R., Souza, A.J., Amoudry, L.O., Plater, A.J., 2016. Effective energy controls on flocculation under various wave-current regimes. Marine Geology 382, 136-150.https://doi.org/10.1016/j.margeo.2016.10.006.

Raunkjær, K., Hvitved-Jacobsen, T., Nielsen, P.H., 1994. Measurement of pools of protein, carbohydrate and lipid in domestic wastewater. Water Research 28, 251-262.https://doi.org/10.1016/0043-1354(94)90261-5.

Razaz, M., Kawanisi, K., Nistor, I., 2015. Tide-driven controls on maximum near-bed floc size in a tidal estuary. Journal Of Hydro-Environment Research 9, 465-471.https://doi.org/10.1016/j.jher.2014.04.001.

Ren, M.E., 1986. Tidal mud flat, Modern Sedimentation in the Coastal and Nearshore Zones of China. China Ocean Press, Beijing, pp. 78–127.

Schwarz, C., Cox, T., van Engeland, T., van Oevelen, D., van Belzen, J., van de Koppel, J., Soetaert, K., Bouma, T.J., Meire, P., Temmerman, S., 2017. Field estimates of floc dynamics and settling velocities in a tidal creek with significant along-channel gradients in velocity and SPM. Estuarine, Coastal and Shelf Science.http://dx.doi.org/10.1016/j.ecss.2017.08.041.

Shao, Y., Yan, Y., Maa Jerome, P.-Y., 2011. In Situ Measurements of Settling Velocity near Baimao Shoal in Changjiang Estuary. Journal of Hydraulic Engineering 137, 372-380.https://doi.org/10.1061/(ASCE)HY.1943-7900.0000312.

Shi, B.W., Yang, S.L., Wang, Y.P., Li, G.C., Li, M.L., Li, P., Li, C., 2017. Role of wind in erosion-accretion cycles on an estuarine mudflat. Journal Of Geophysical Research-Oceans 122, 193-206.https://doi.org/10.1002/2016jc011902.

Soulsby, R., 1997. Dynamics of marine sands : a manual for practical applications. Thomas Telford, London.

Soulsby, R.L., Dyer, K.R., 1981. The form of the near-bed velocity profile in a tidally accelerating flow. Journal of Geophysical Research: Oceans 86, 8067-8074.http://dx.doi.org/10.1029/JC086iC09p08067.
Soulsby, R.L., Humphery, J.D., 1990. Field Observations of Wave-Current Interaction at the Sea Bed, in: Tørum, A., Gudmestad, O.T. (Eds.), Water Wave Kinematics. Springer Netherlands, Dordrecht, pp. 413-428.
Soulsby, R.L., Manning, A.J., Spearman, J., Whitehouse, R.J.S., 2013. Settling velocity and mass settling flux of flocculated estuarine sediments. Marine Geology 339, 1-12.https://doi.org/10.1016/j.margeo.2013.04.006.
Tan, X.-l., Zhang, G.-p., Yin, H., Reed, A.H., Furukawa, Y., 2012. Characterization of particle size and settling velocity of cohesive sediments affected by a neutral exopolymer. International Journal Of Sediment Research 27, 473-485.https://doi.org/10.1016/S1001-6279(13)60006-2.
Tran, D., Kuprenas, R., Strom, K., 2018. How do changes in suspended sediment concentration alone influence the size of mud flocs under steady turbulent shearing? Continental Shelf Research 158, 1-14.https://doi.org/10.1016/j.csr.2018.02.008.
Tsai, C.-H., Iacobellis, S., Lick, W., 1987. Flocculation of Fine-Grained Lake Sediments Due to a Uniform Shear Stress. Journal of Great Lakes Research 13, 135-146.https://doi.org/10.1016/S0380-1330(87)71637-2.
Van der Lee, W.T.B., 2000. Temporal variation of floc size and settling velocity in the Dollard estuary. Continental Shelf Research 20, 1495-1511.https://doi.org/10.1016/S0278-4343(00)00034-0.
Van Leussen, W., 1988. Aggregation of Particles, Settling Velocity of Mud Flocs A Review, in: Dronkers, J., van Leussen, W. (Eds.), Physical Processes in Estuaries. Springer Berlin Heidelberg, Berlin, Heidelberg, pp. 347-403.
Van Leussen, W., 1994. Estuarine Macroflocs and Their Role in Fine-Grained Sediment Transport. Ph. D. Thesis, University of Utrecht.
Wang, Y.P., Gao, S., Jia, J.J., 2006. High-resolution data collection for analysis of sediment dynamic processes associated with combined current-wave action over intertidal flats. Chinese Science Bulletin 51, 866-877.https://doi.org/10.1007/s11434-006-0866-1.
Wang, Y.P., Gao, S., Jia, J.J., Thompson, C.E.L., Gao, J.H., Yang, Y., 2012. Sediment transport over an accretional intertidal flat with influences of reclamation, Jiangsu coast, China. Marine Geology 291, 147-161.https://doi.org/10.1016/j.margeo.2011.01.004.
Wang, Y.P., Gao, S., Ke, X.K., 2004. Observations of boundary layer parameters and suspended sediment transport over the intertidal flats of northern Jiangsu, China. Acta Oceanologica Sinica 23, 437-448.
Wang, Y.P., Voulgaris, G., Li, Y., Yang, Y., Gao, J.H., Chen, J., Gao, S., 2013. Sediment resuspension, flocculation, and settling in a macrotidal estuary. Journal Of Geophysical Research-Oceans 118, 5591-5608.https://doi.org/10.1002/jgrc.20340.
Wells, J.T., 1989. In Situ Measurements of Large Aggregates Over A Fluid Mud Bed. Journal Of Coastal Research, 75-86.
Wendling, V., Gratiot, N., Legout, C., Droppo, I.G., Coulaud, C., Mercier, B., 2015. Using an optical settling column to assess suspension characteristics within the free, flocculation,

and hindered settling regimes. Journal of Soils and Sediments 15, 1991-2003.https://doi.org/10.1007/s11368-015-1135-1.

Williams, J.J., Bell, P.S., Thorne, P.D., 2003. Field measurements of flow fields and sediment transport above mobile bed forms. Journal of Geophysical Research Oceans 108, 3109.https://doi.org/10.1029/2002JC001336.

Winterwerp, J.C., 1998. A simple model for turbulence induced flocculation of cohesive sediment. Journal of Hydraulic Research 36, 309-326.https://doi.org/10.1080/00221689809498621.

Wolanski, E., Gibbs, R.J., Yoshihiro, M., Ashish, M., King, B., 1992. The Role of Turbulence in the Settling of Mud Flocs. Journal Of Coastal Research 8, 35-46.

Wotton, R.S., 2004. The utiquity and many roles of exopolymers (EPS) in aquatic systems. Scientia Marina 68, 9.https://doi.org/10.3989/scimar.2004.68s113.

Wotton, R.S., 2005. The Essential Role of Exopolymers (Eps) in Aquatic Systems, in: Gibson, R.N., Atkinson, R.J.A., Gordon, J.D.M. (Eds.), Oceanography and Marine Biology: An Annual Review, 1st ed. CRC Press, Boca Raton, pp. 57-94.

Xing, F., Wang, Y.P., Wang, H.V., 2012. Tidal hydrodynamics and fine-grained sediment transport on the radial sand ridge system in the southern Yellow Sea. Marine Geology 291–294, 192-210.https://doi.org/10.1016/j.margeo.2011.06.006.

Xiong, J., Wang, X.H., Wang, Y.P., Chen, J., Shi, B., Gao, J., Yang, Y., Yu, Q., Li, M., Yang, L., Gong, X., 2017. Mechanisms of maintaining high suspended sediment concentration over tide-dominated offshore shoals in the southern Yellow Sea. Estuarine, Coastal and Shelf Science 191, 221-233.https://doi.org/10.1016/j.ecss.2017.04.023.

Zhang, Q., Gong, Z., Zhang, C., Zhou, Z., Townend, I., 2016. Hydraulic and Sediment Dynamics at times of Very Shallow Water on Intertidal Mudflats: The Contribution of Waves. Journal Of Coastal Research, 507-511.https://doi.org/10.2112/SI75-102.1.

Zhao, Y.Y., Gao, S., 2015. Simulation of Tidal Flat Sedimentation in Response to Typhoon-induced Storm Surges: A case study from Rudong Coast,Jiangsu,China. Acta Sedimentologica Sinica.https://doi.org/10.14027/j.cnki.cjxb.2015.01.008.

Figure captions

Fig. 1 Maps showing the study area and the location of the intertidal flats at Rudong, Jiangsu, China (b: on the basis of a 2016 Landsat8 TM image). In (a), blue lines indicate the bathymetric contours (m) referenced to the lowest low water datum. In (b), red dots indicate the location of observation sites. Site S1 was located in a clam aquaculture region, while Site S2 was located on a bare tidal flat.

Fig. 2 Relationships between SSC (suspended sediment concentration of in situ water samples) and T (Turbidity recorded by OBS-3A) for Site S1 (a) and S2 (b). R denotes correlation coefficient and N indicates the number of data paris.

Fig. 3 (a) Vertical profiles of extracellular polymeric substances (EPS, $\mu g\ g^{-1}\ DW$) content of field sediment cores. (b) Cumulative content of extracellular polymeric substances (EPS, $\mu g\ g^{-1}\ DW$) in vertical profiles of field sediment cores. Error bars in (a) indicate the standard deviation of the EPS content.

Fig. 4 Observations of (a) water depth (m), (b) wave height (m), (c) current velocity (m s^{-1}), (d) bed shear stress (N m^{-2}), (e) maximum bed shear stress for combined waves and currents (N m^{-2}).

Fig. 5 Temporal variability of (a) velocity (m s^{-1}) and water depth (m), (b) mean size (μm) of in situ suspended particles, (c) suspended sediment concentration (g L^{-1}) and volume concentration (VC, μl L^{-1}), (d) shear rate (G_{CW}^{-m}, s^{-1}), (e) Effective density (kg m^{-3}), and (f) distance from probe to bed (mm) for Site S1 and S2, respectively.

Fig. 6 Comparison of Particle size distributions measured in the lab with a Malvern Master Sizer (2-2000 μm) and in-situ with a LISST (2.5-500 μm) over the measured tide.

Fig. 7 Time series of in situ particles size distribution for (a) Site S1, and (b) Site S2

Fig. 8 Relation between variations of effective density and in situ mean particle size

Fig. 9 Scatter plots between in situ mean particle size (D_M, μm) with SSC (g L^{-1}) for Site S1 with clam and Site S2, respectively.

Fig. 10 Relationships between tidally-averaged in situ mean size (D_M, μm) and SSC (g L^{-1}), shear rate G_{u*} (s^{-1}), shear rate G_{CW} (s^{-1}), and SSC·G_{CW} (g m^{-3} s^{-1}) for Site S1 with clam (a), (c), (e), (g), and Site S2 (b) , (d), (f), (h), respectively.

Fig. 11 Relationships between total shear stress (τ_{cw_max}, N m^{-2}) and suspended sediment concentration (SSC, g L^{-1}) for Site S1 with clam (a) and Site S2 (b), respectively.

Table headings

Table 1 Statistics of hydrodynamic conditions including wave height (Hs, m), current speed (m s^{-1}), bed shear stress due to waves (τ_w, N m^{-2}) and currents (τ_c, N m^{-2}), the combined shear stress due to wave and currents (τ_{cw_max}, N m^{-2}), suspended sediment concentration (SSC, g L^{-1}), in situ mean particle size (D_M, μm), effective density ($\Delta\rho$, kg m^{-3}) and shear rate (G, s^{-1}).

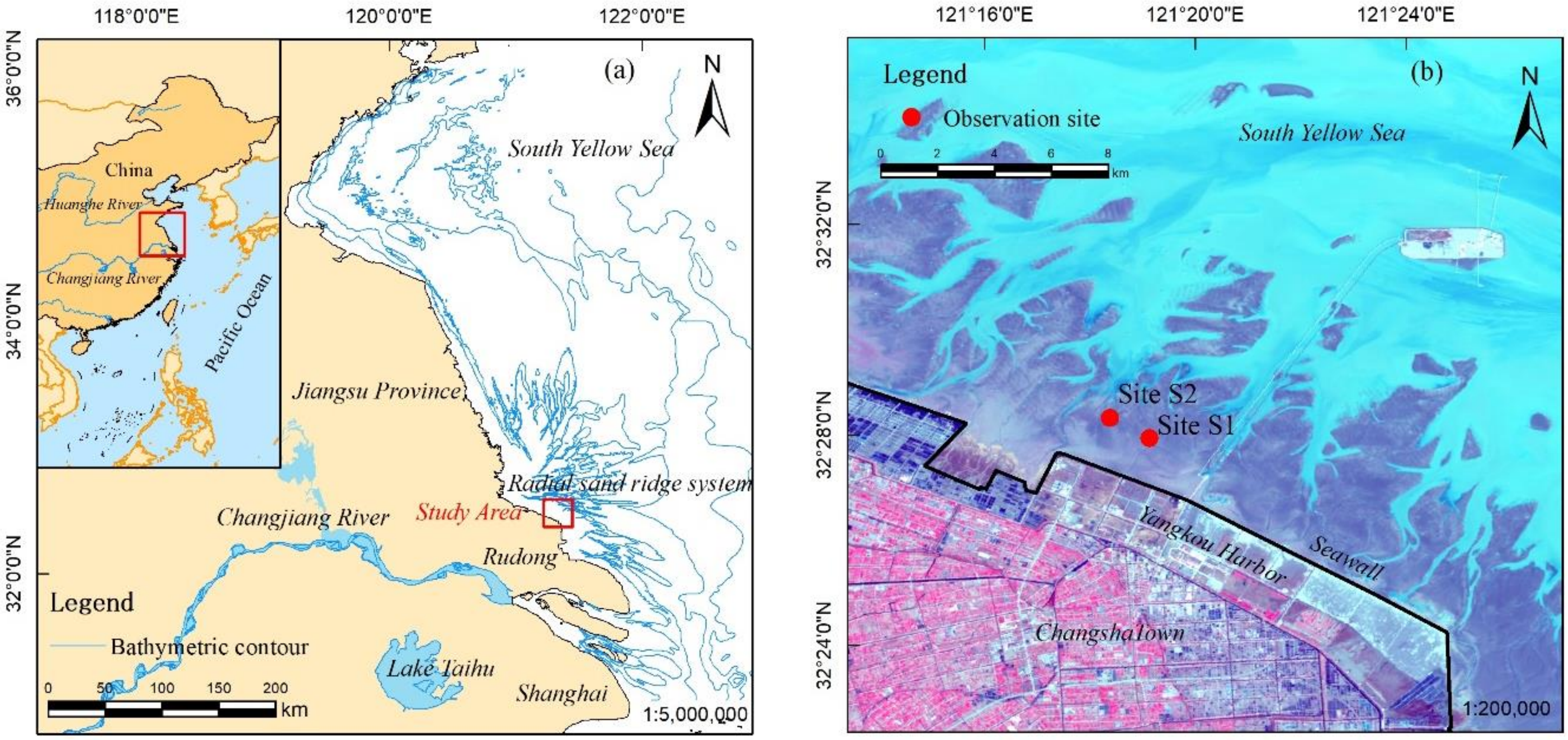

Fig. 1 Maps showing the study area and the location of the intertidal flats at Rudong, Jiangsu, China (b: on the basis of a 2016 Landsat8 TM image). In (a), blue lines indicate the bathymetric contours (m) referenced to the lowest low water datum. In (b), red dots indicate the location of observation sites. Site S1 was located in a clam aquaculture region, while Site S2 was located on a bare tidal flat.

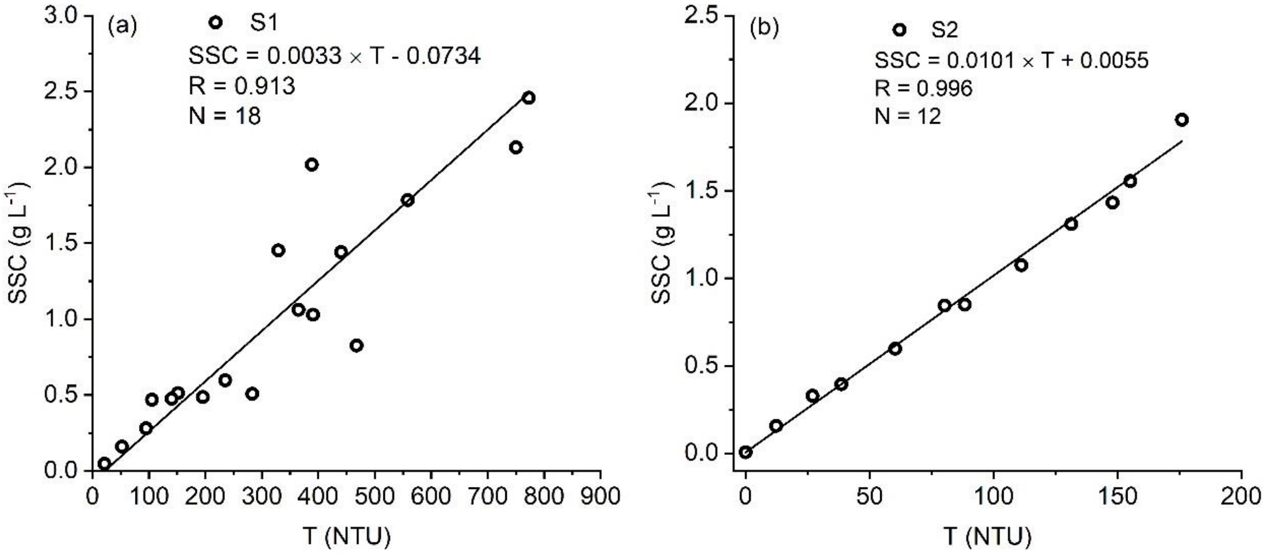

Fig. 2 Relationships between SSC (suspended sediment concentration of in situ water samples) and T (Turbidity recorded by OBS-3A) for Site S1 (a) and S2 (b). R denotes the correlation coefficient and N indicates the number of data pairs.

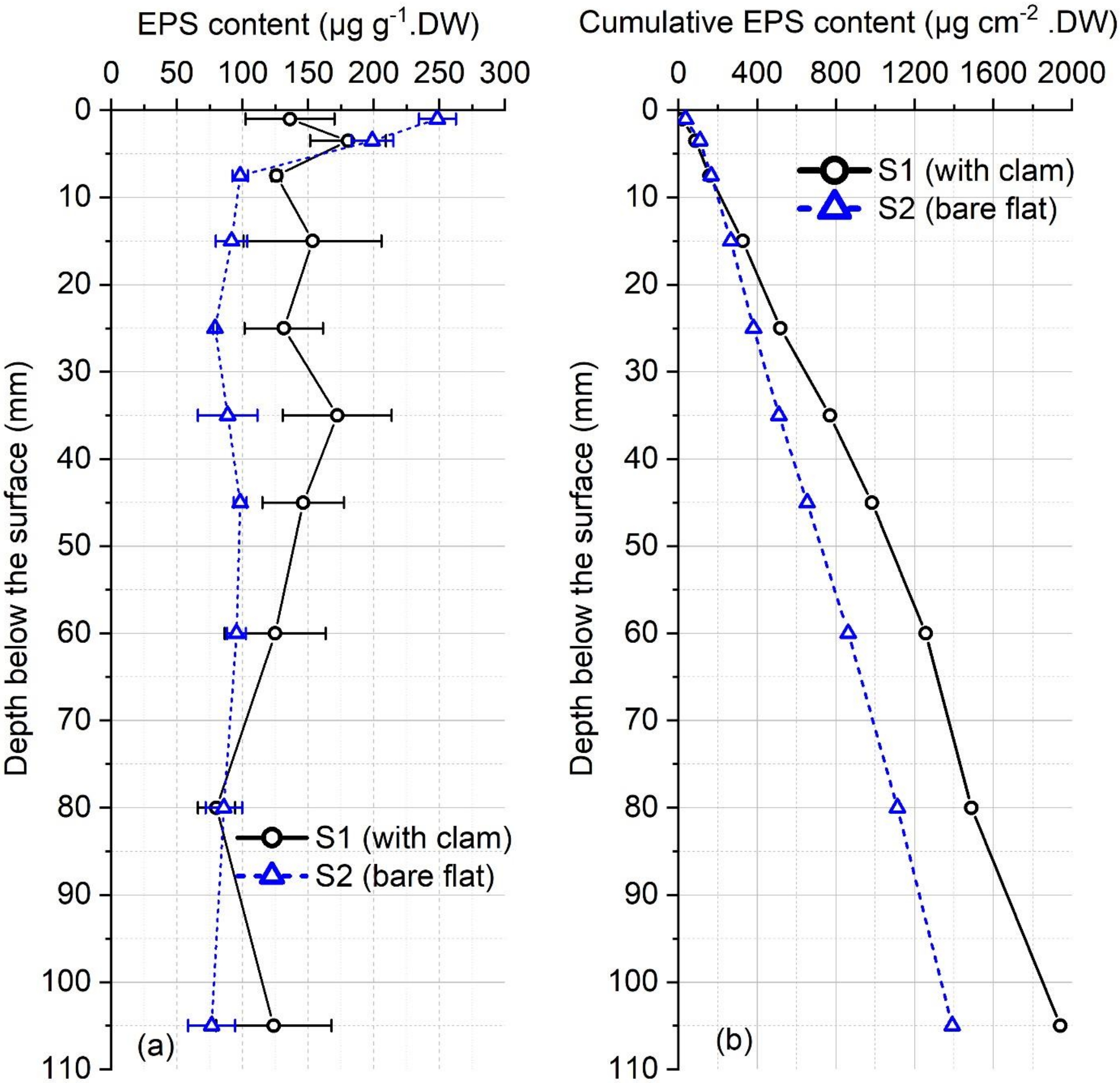

Fig. 3 (a) Vertical profiles of extracellular polymeric substances (EPS, $\mu g\ g^{-1}\ DW$) content of field sediment cores. (b) Cumulative content of extracellular polymeric substances (EPS, $\mu g\ cm^{-2}\ DW$) in vertical profiles of field sediment cores. Error bars in (a) indicate the standard deviation of the EPS content.

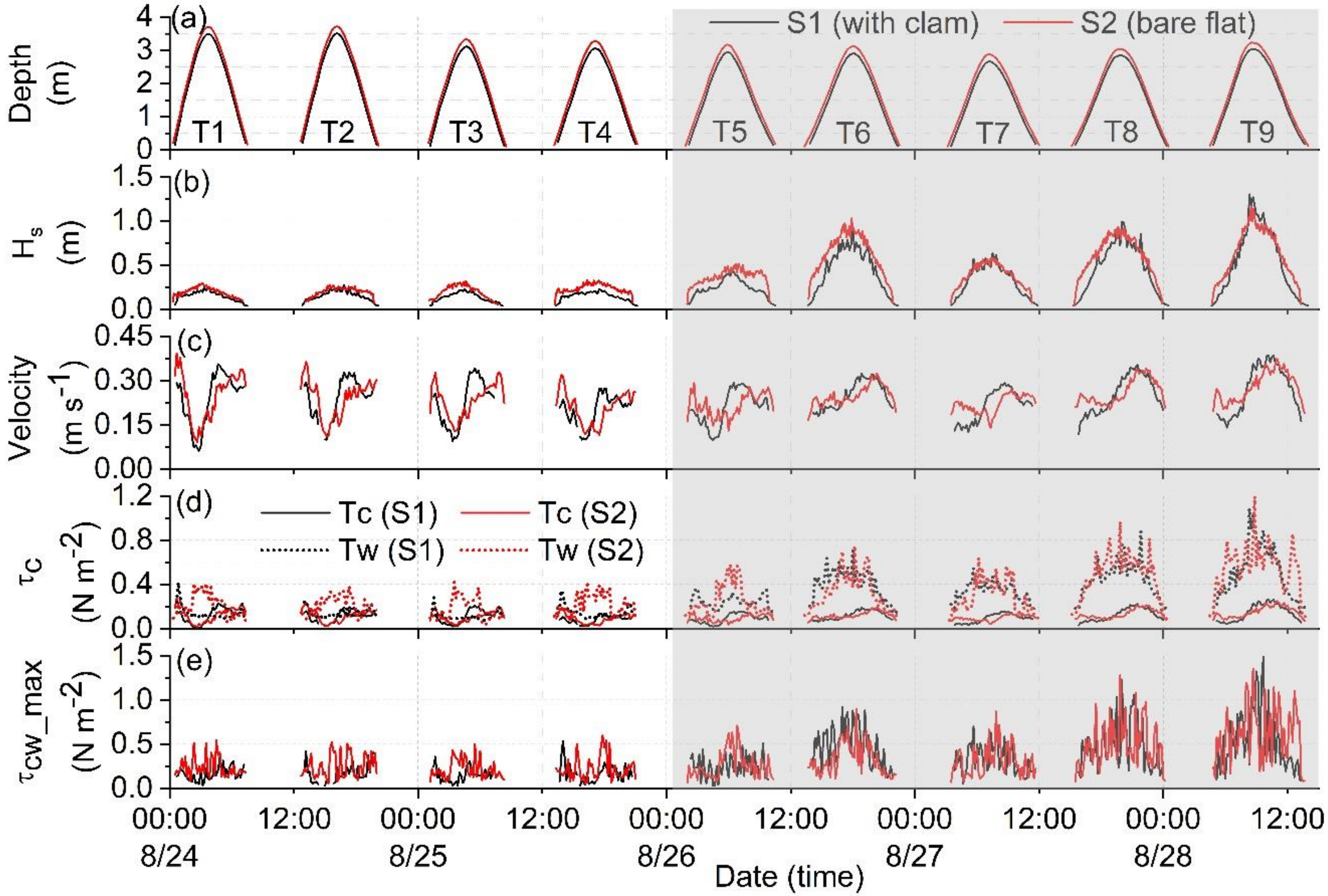

Fig. 4 Observations of (a) water depth (m), (b) wave height (m), (c) current velocity (m s^{-1}), (d) bed shear stress (N m^{-2}), (e) maximum bed shear stress for combined waves and currents (N m^{-2}).

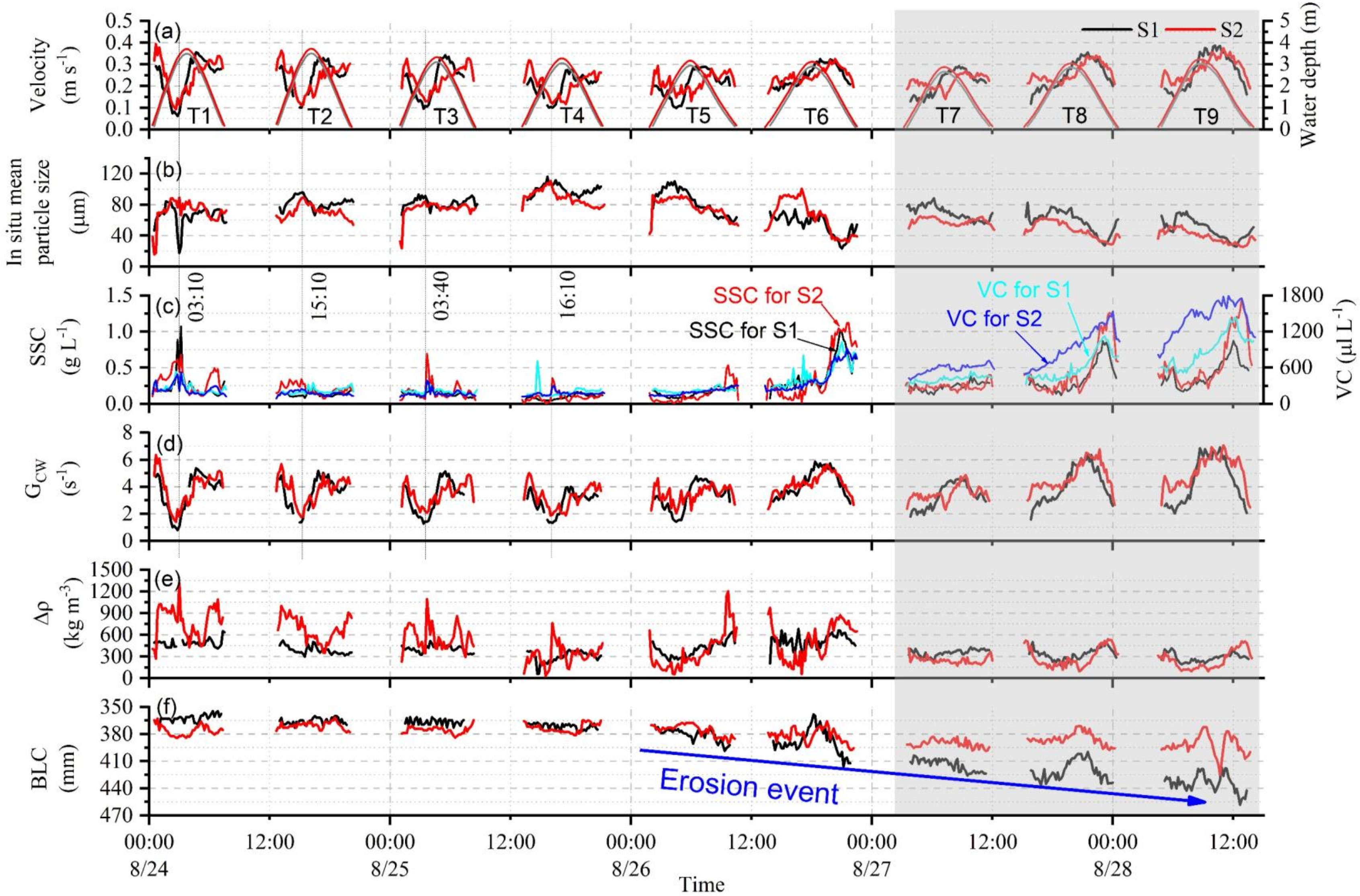

Fig. 5 Temporal variability of (a) Velocity (m s^{-1}) and water depth (m), (b) Mean size (μm) of in situ suspended particles, (c) Suspended sediment concentration (g L^{-1}) and volume concentration (VC, μl L^{-1}), (d) Shear rate (G_{CW}, s^{-1}), (e) Effective density (kg m^{-3}), and (f) Distance from the probe to bed (mm) for Site S1 (with clam) and S2 (bare flat), respectively.

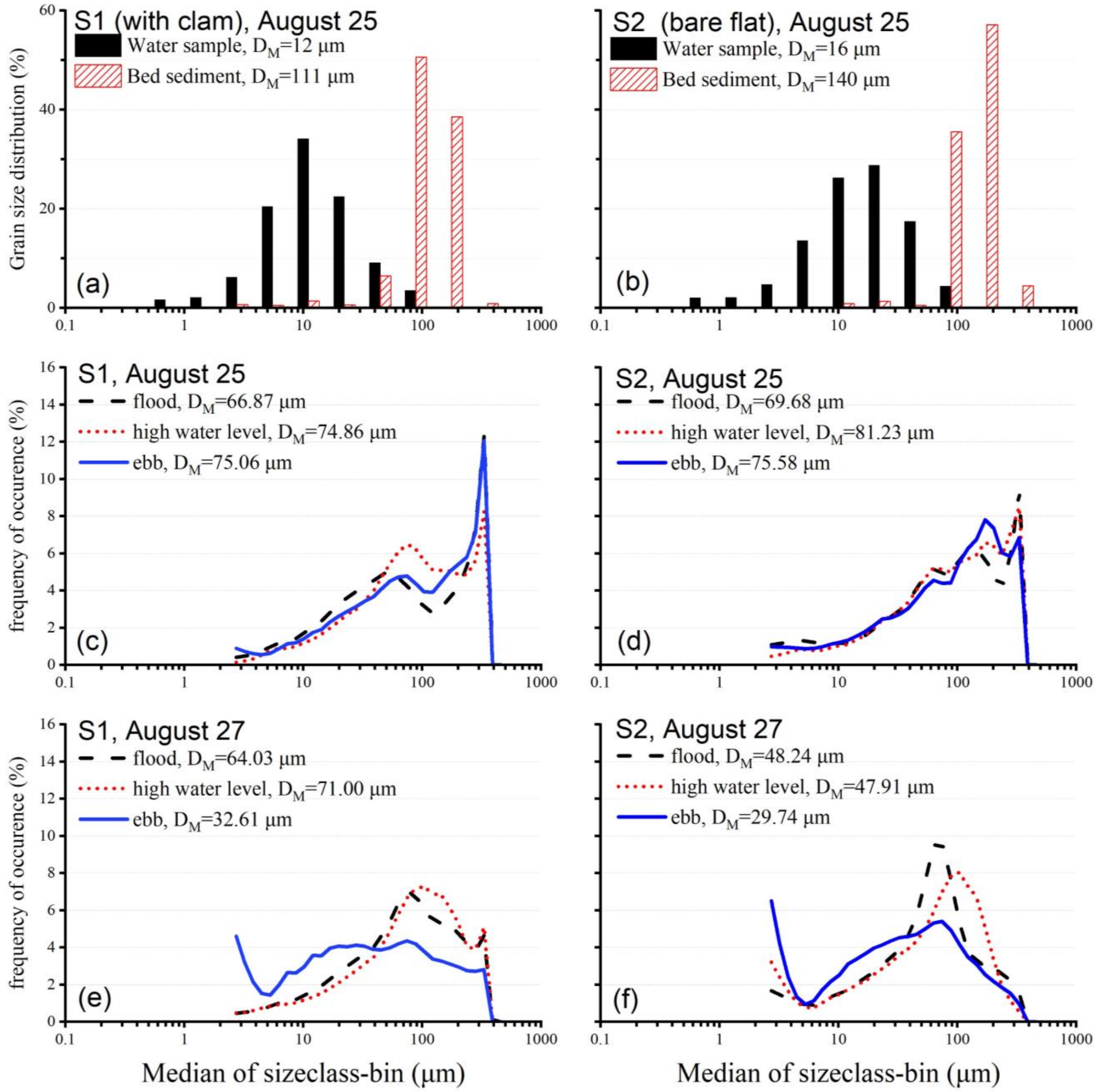

Fig. 6 Comparison of Particle size distributions measured in the lab with a Malvern Master Sizer (2-2000 μm) and in-situ with a LISST (2.5-500 μm) over the measured tide.

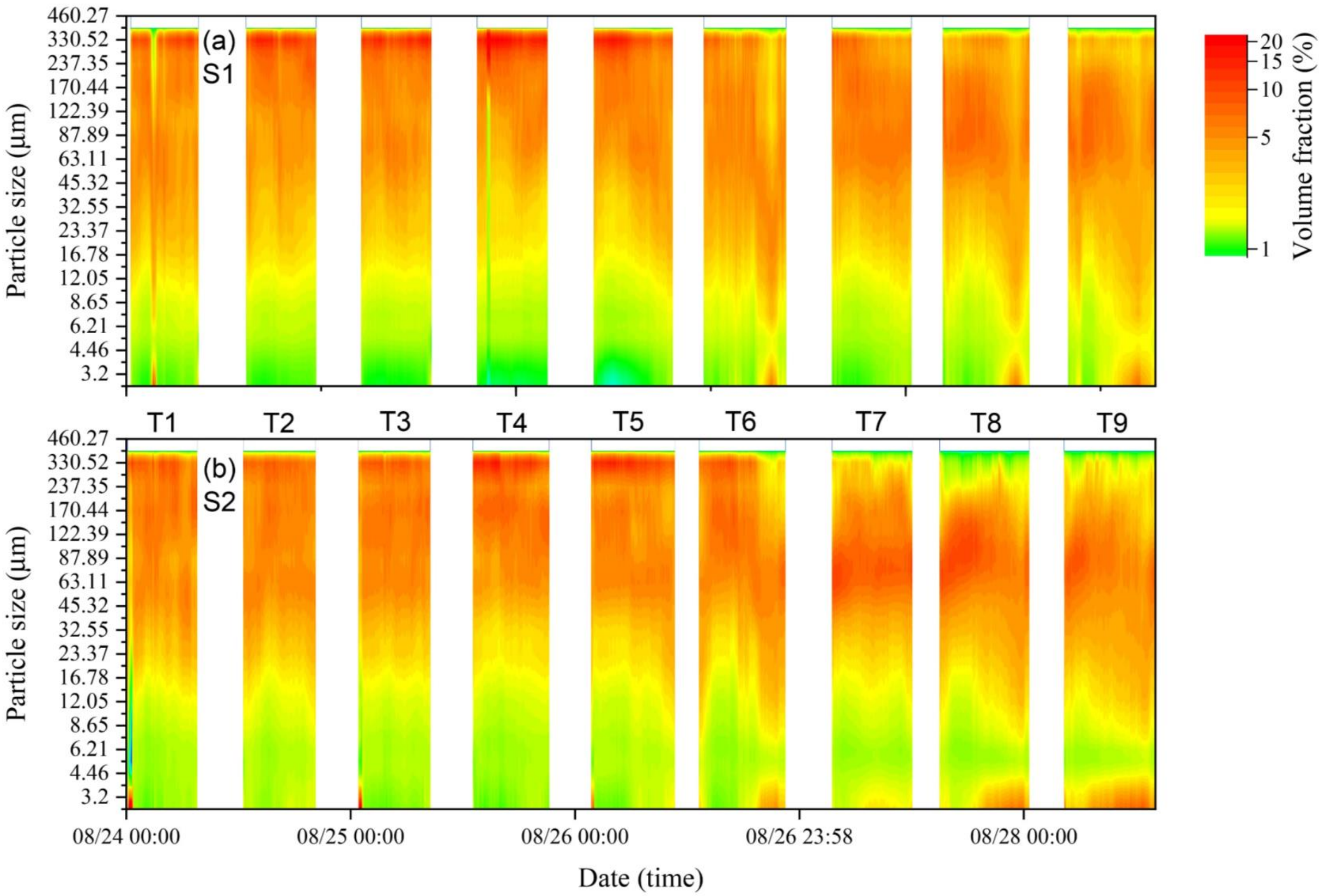

Fig. 7 Time series of in situ particle size distribution for (a) Site S1, and (b) Site S2.

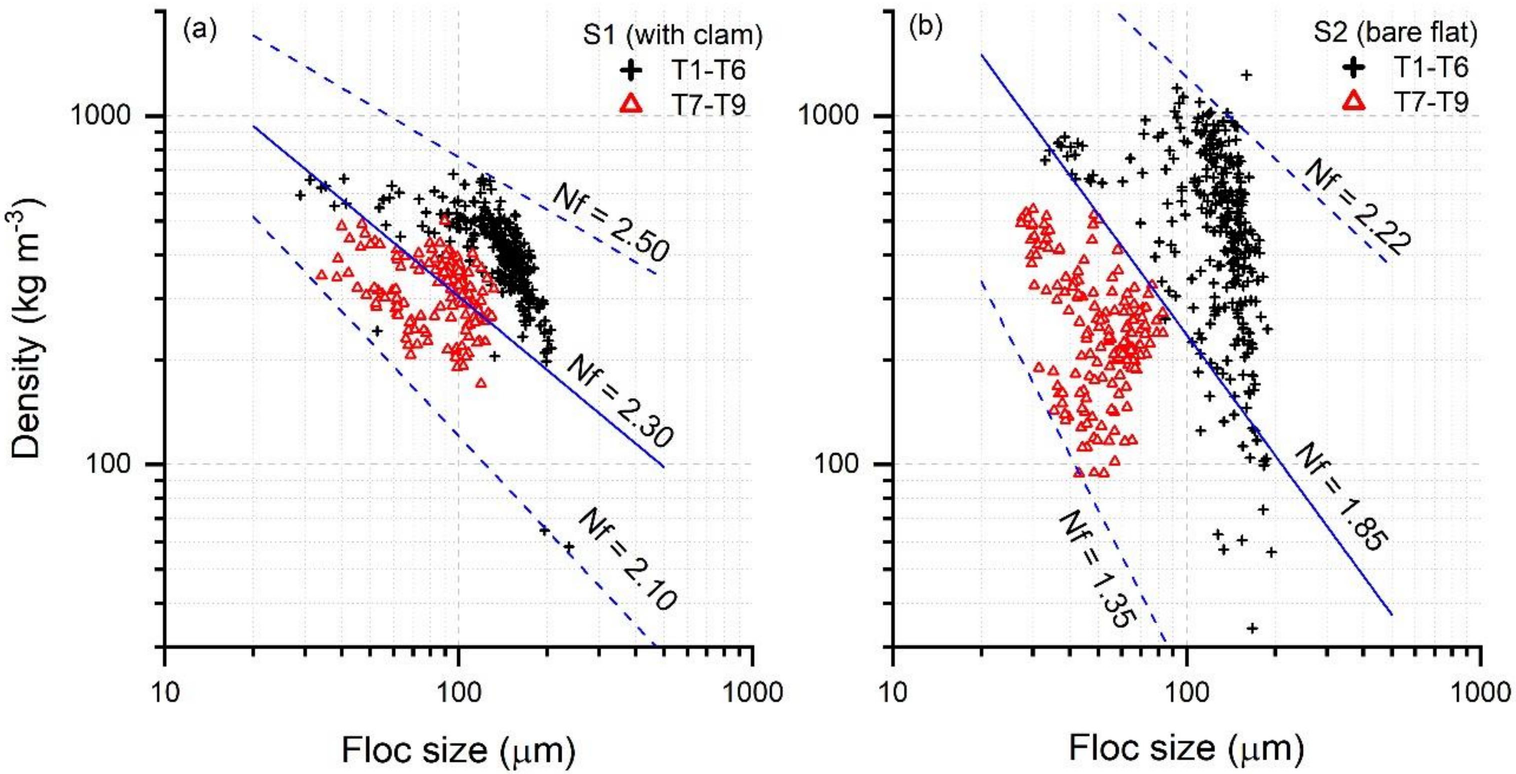

Fig. 8 Relation between variations of effective density and in situ mean particle size.

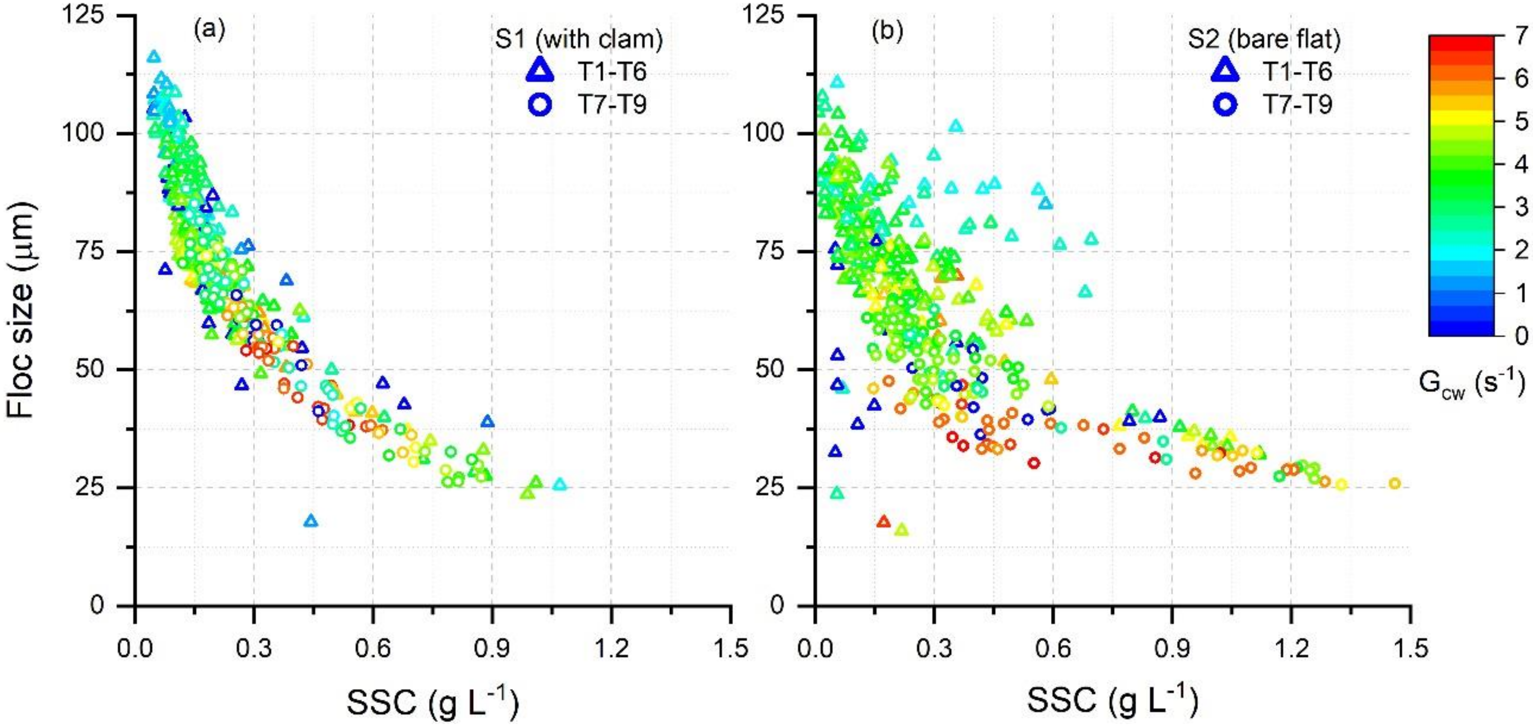

Fig. 9 Scatter plots between in situ mean particle size (D_M, μm) with SSC (g L^{-1}) for Site S1 (with clam) and Site S2 (bare flat), respectively.

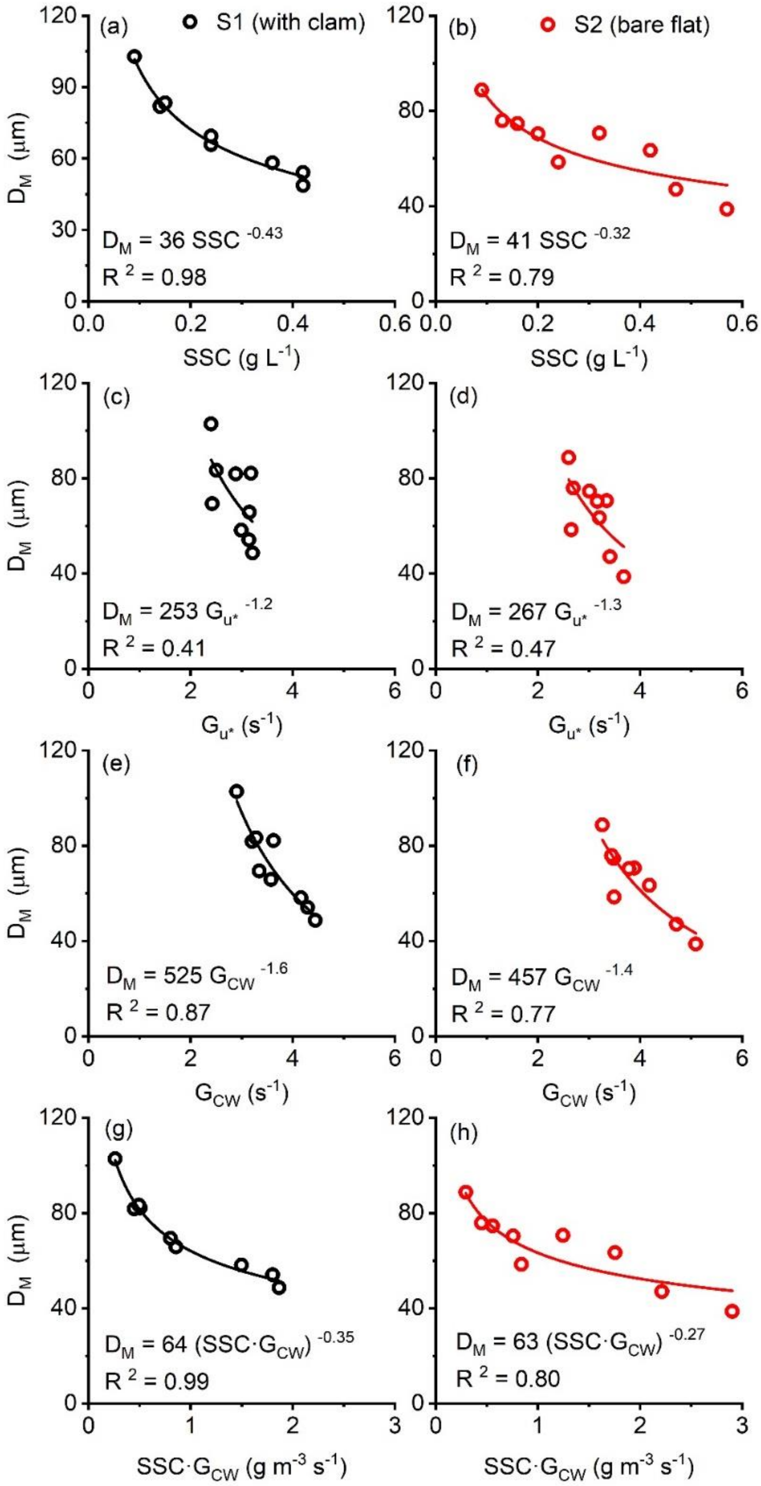

Fig. 10 Relationships between tidally-averaged in situ mean size (D_M, μm) and SSC (g L^{-1}), shear rate G_{u*} (s^{-1}), shear rate G_{CW} (s^{-1}), and SSC·G_{CW} (g m^{-3} s^{-1}) for Site S1 with clam (a), (c), (e), (g), and Site S2 at bare flat (b) , (d), (f), (h), respectively.

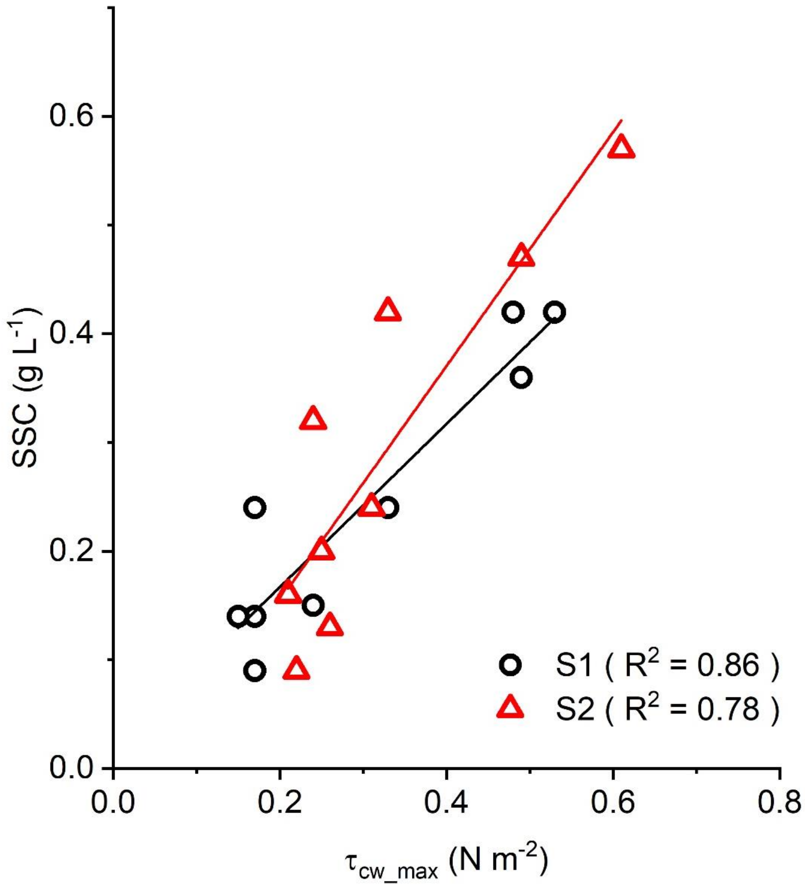

Fig. 11 Relationships between total shear stress (τ_{cw_max}, N m^{-2}) and suspended sediment concentration (SSC, g L^{-1}) for Site S1 with clam and Site S2 at the bare flat.

Table 1 Statistics of hydrodynamic conditions including wave height (Hs, m), current speed (m s^{-1}), bed shear stress due to waves (τ_w, N m^{-2}) and currents (τ_c, N m^{-2}), the combined shear stress due to wave and currents (τ_{cw_max}, N m^{-2}), suspended sediment concentration (SSC, g L^{-1}), in situ mean particle size (D_M, μm), effective density (Δρ, kg m^{-3}) and shear rate (G, s^{-1}).

Station	Tide	Hs m	Speed m s^{-1}	τ_w N m^{-2}	τ_c N m^{-2}	τ_{cw_max} N m^{-2}	SSC g L^{-1}	Mz μm	Δρ kg m^{-3}	G_{cw} s^{-1}	G_{u*} s^{-1}
S1	T1	0.15	0.24	0.14	0.12	0.17	0.24	65.85	488.02	3.57	3.15
	T2	0.15	0.24	0.14	0.12	0.17	0.14	82.19	386.80	3.62	3.18
	T3	0.14	0.22	0.11	0.11	0.15	0.14	81.89	409.91	3.20	2.88
	T4	0.15	0.20	0.15	0.08	0.17	0.09	102.87	298.80	2.90	2.40
	T5	0.24	0.21	0.24	0.09	0.24	0.15	83.44	401.03	3.28	2.50
	T6	0.44	0.25	0.40	0.12	0.48	0.42	54.19	515.94	4.29	3.14
	T7	0.32	0.22	0.34	0.09	0.33	0.24	69.44	352.83	3.34	2.42
	T8	0.47	0.25	0.45	0.13	0.49	0.36	58.28	335.42	4.16	2.99
	T9	0.53	0.27	0.50	0.15	0.53	0.42	48.74	285.54	4.44	3.21
S2	T1	0.20	0.25	0.21	0.13	0.24	0.32	70.70	776.73	3.89	3.34
	T2	0.21	0.24	0.22	0.12	0.25	0.20	70.40	681.52	3.78	3.16
	T3	0.20	0.23	0.17	0.11	0.21	0.16	74.66	564.59	3.48	3.01
	T4	0.24	0.21	0.22	0.09	0.22	0.09	88.77	318.70	3.26	2.60
	T5	0.37	0.22	0.25	0.10	0.26	0.13	75.98	368.16	3.44	2.69
	T6	0.38	0.25	0.33	0.12	0.33	0.42	63.49	505.42	4.18	3.20
	T7	0.31	0.22	0.29	0.10	0.31	0.24	58.51	248.60	3.49	2.65
	T8	0.48	0.26	0.48	0.13	0.49	0.47	47.13	286.89	4.71	3.41
	T9	0.51	0.28	0.53	0.15	0.61	0.57	38.74	248.74	5.09	3.68

We confirm we have no conflict of interest.